

Naval Research Laboratory

Washington, DC 20375-5000



NRL Memorandum Report 6365

Chaotic Electron Motion Caused by Sidebands in Free Electron Lasers

S. RIYOPOULOS

*Science Applications Intl. Corp.
McLean, VA 22102*

C. M. TANG

*Plasma Theory Branch
Plasma Physics Division*

October 27, 1988

DTIC
ELECTE
DEC 09 1988
S D H

SECURITY CLASSIFICATION OF THIS PAGE

REPORT DOCUMENTATION PAGE				Form Approved OMB No 0704-0188	
1a REPORT SECURITY CLASSIFICATION UNCLASSIFIED			1b RESTRICTIVE MARKINGS		
2a SECURITY CLASSIFICATION AUTHORITY			3 DISTRIBUTION/AVAILABILITY OF REPORT Approved for public release; distribution unlimited.		
2b DECLASSIFICATION/DOWNGRADING SCHEDULE					
4 PERFORMING ORGANIZATION REPORT NUMBER(S) NRL Memorandum Report 6365			5 MONITORING ORGANIZATION REPORT NUMBER(S)		
6a NAME OF PERFORMING ORGANIZATION Naval Research Laboratory		6b OFFICE SYMBOL (If applicable) Code 4790		7a NAME OF MONITORING ORGANIZATION	
6c ADDRESS (City, State, and ZIP Code) Washington, DC 20375-5000		7b ADDRESS (City, State, and ZIP Code)			
8a NAME OF FUNDING/SPONSORING ORGANIZATION Strategic Defense Initiative Org.		8b OFFICE SYMBOL (If applicable)		9 PROCUREMENT INSTRUMENT IDENTIFICATION NUMBER	
8c ADDRESS (City, State, and ZIP Code) Washington, DC 20301-7100		10 SOURCE OF FUNDING NUMBERS			
		PROGRAM ELEMENT NO 63221C		PROJECT NO W31RPD-7-D4039	
		TASK NO		WORK UNIT ACCESSION NO	
11 TITLE (Include Security Classification) Chaotic Electron Motion Caused by Sidebands in Free Electron Lasers					
12 PERSONAL AUTHOR(S) Riyopoulos,* S. and Tang, C. M.					
13a TYPE OF REPORT Interim		13b TIME COVERED FROM _____ TO _____		14 DATE OF REPORT (Year, Month, Day) 1988 October 27	
				15 PAGE COUNT 87	
16 SUPPLEMENTARY NOTATION *Science Application Intl. Corp., McLean, VA 22102					
17 COSATI CODES			18 SUBJECT TERMS (Continue on reverse if necessary and identify by block number)		
FIELD	GROUP	SUB-GROUP	FELs Detrapping		
			Sidebands Stochasticity		
19 ABSTRACT (Continue on reverse if necessary and identify by block number)					
<p>The electron dynamics in a Free Electron Laser (FEL) is studied in the case when the radiation field contains many modes. This situation arises when unstable modes (sidebands) are excited during operation. It is observed that when the strength of these sidebands exceeds certain levels, the electron motion becomes chaotic. This may lead to extensive particle detrapping and loss of amplification for the FEL signal. The threshold for the onset of stochastic electron motion is computed. The evolution of the trapped electron distribution exhibits a diffusive behavior. The rate of particle detrapping is parameterized by the diffusion coefficient D in action space. The e-folding length for the number of trapped electrons is parametrized by J_s^2/D where J_s is the action at the separatrix. It is found that the diffusion rates are connected to the type of the sideband spectrum. The diffusion coefficient is always proportional to the ratio of the sideband power in all</p> <p style="text-align: right;">(Continues)</p>					
20 DISTRIBUTION AVAILABILITY OF ABSTRACT <input checked="" type="checkbox"/> UNCLASSIFIED/UNLIMITED <input type="checkbox"/> SAME AS RPT <input type="checkbox"/> DTIC USERS			21 ABSTRACT SECURITY CLASSIFICATION UNCLASSIFIED		
22a NAME OF RESPONSIBLE INDIVIDUAL C.M. Tang			22b TELEPHONE (Include Area Code) (202) 767-4248		22c OFFICE SYMBOL Code 4790

DD Form 1473, JUN 86

Previous editions are obsolete

SECURITY CLASSIFICATION OF THIS PAGE

S/N 0102-LF-014-6603

19. ABSTRACTS (Continued)

frequencies to the power of the carrier signal. The coefficient of the proportionality however scales differently on the FEL parameters for each of the three spectral categories: a narrow, a broad discrete and a broad continuous spectrum. The diffusion coefficient is computed analytically for the last two cases and is in good agreement with numerical results. The narrow spectrum yields the highest and the broad continuous the lowest diffusion rates under constant sideband power. It is also found that, in all cases, the diffusion length, measured in wiggler periods, is independent of the electron energy γ .

CONTENTS

I.	INTRODUCTION	1
II.	GENERAL CONSIDERATIONS	6
III.	PORTRAIT OF THE PHASE SPACE	10
IV.	THRESHOLD FOR ERRATIC MOTION	15
V.	NARROW FREQUENCY BAND DIFFUSION	19
VI.	BROAD FREQUENCY BAND DIFFUSION	22
	A. Broad Discrete Spectrum	24
	B. Broad Continuous Spectrum	27
VII.	NUMERICAL RESULTS	33
VIII.	CONCLUSION	36
	ACKNOWLEDGEMENT	37
	APPENDIX A — Transformations in Action-Angle Variables	39
	APPENDIX B — Phase Averaging Over Constant J	43
	APPENDIX C — Computation of the Quasilinear Diffusion Coefficient	45
	APPENDIX D — Summation of Fourier Coefficients	49
	REFERENCES	52
	DISTRIBUTION LIST	67

CHAOTIC ELECTRON MOTION CAUSED BY SIDEBANDS IN FREE ELECTRON LASERS

I. INTRODUCTION

Multifrequency effects in Free Electron Lasers (FELs) become increasingly important as progress is made towards high power operation. Growth of parasitic frequencies (sidebands¹⁻⁵) has been predicted theoretically and has been observed in experiments^{6,7} as well as in simulations⁸⁻¹¹ with either constant or tapered wigglers¹¹. The efficiency for the carrier signal is reduced and the optical quality is degraded as power is channeled into frequencies apart from the intended operation frequency. Another potential hazard that has attracted little attention so far is the onset of chaotic electron motion caused by the presence of even a single frequency sideband. This may lead to extensive particle detrapping and premature loss of the amplification for all the radiation modes independent of frequency.

Two of the main issues concerning FEL operation are: (a) whether unstable parasitic frequencies exist that can grow to significant amplitude and (b) what is the effect of potentially unstable modes on the trapped electron trajectories. Considerable attention has been devoted to the linear stability issue. The gain for small sideband signal has been computed analytically¹⁻⁵ invoking either ensemble averaging over single particle trajectories or solutions of the perturbed kinetic equation for the distribution function. Initial results, obtained for particles localized near the bottom of the ponderomotive well, and, in particular, more recent results including all trapped and untrapped particles² with arbitrary distributions, have demonstrated that every nontrivial distribution $df_0/dJ \neq 0$ is unstable to sideband growth.

Given that sidebands cannot be eliminated, the growth of the unstable modes to a finite amplitude may have serious effects on the unperturbed trajectories. It has been known that stochastic behavior¹² is an intrinsic property of perturbed Hamiltonian systems^{13,14}. Accordingly, the electron motion in a FEL will become chaotic when the sideband amplitude exceeds a certain threshold. This, in turn, will result in significant electron detrapping. Since it is the deceleration of the trapped electron bucket that provides the energy for the radiation in case of tapered wigglers, detrapping will cause loss of amplification for the FEL signal.

In the present work we investigate the nonlinear effects caused by sidebands. The threshold for stochasticity, above which unbound chaotic motion occurs, is determined. Once the stochastic transition takes place, the action J , a constant of motion in the unperturbed system, changes in a random manner. The ensemble average $\langle \Delta X^2 \rangle$ of any physical quantity X is described by a diffusion equation. Diffusion of the action invariant provides a measure of the leakage rate across the separatrix. If D is the effective diffusion coefficient in action space then the diffusion length $L_d = J_s^2/D$, where J_s is the action at the separatrix, signifies the length over which approximately half of the deeply trapped particles get detrapped. We show that a single frequency sideband at a modest fraction of the carrier amplitude suffices to spread irregular motion over a significant fraction of the trapped particle domain. However, given that the interaction time of an electron in a FEL is short, we are mainly concerned on how fast this diffusion occurs. The diffusion rate increases and the diffusion length L_d decreases with increasing sideband amplitude(s). Thus, a critical sideband level a_c can be defined above which the diffusion length L_d

becomes shorter than the wiggler length L_w . Obviously the power level for the sidebands in a FEL cannot exceed a_c , otherwise, extensive diffusion and premature detrapping will occur. On the other hand, enough electrons can remain trapped during the interaction period even though their motion has turned stochastic, because we find that usually the critical amplitude a_c is much larger than the threshold for stochasticity α_s .

A clear-cut relation between the diffusion rate under constant total sideband power and the type of the excited sideband spectrum is discovered. More specifically we observe three regimes in the simulation parameters defining the sideband spectrum, corresponding to a narrow, a wide discrete and a wide continuous spectrum. The transition from one spectral type to another is accompanied by an abrupt change in the diffusion rates. In all cases we find the diffusion coefficient proportional to the ratio of the total power in the sidebands to the FEL carrier power. The coefficients of this proportionality depend on the spectral type. A general conclusion is that the diffusion rate under constant sideband power ratio decreases with increasing number of spectral components. The diffusion rate for a single sideband frequency exceeds that of a broad continuous spectrum by orders of magnitude while a broad discrete spectrum causes intermediate diffusion rates.

For practical purposes we measure the diffusion length in terms of the number of wiggler periods, $N_d = l_d/\lambda_w$, while $\langle \Delta I^2 \rangle$ is normalized to the action J_s at the (unperturbed) separatrix. We compute the normalized diffusion coefficient D analytically for the cases of broad discrete and continuous spectra. In the latter case the quasilinear diffusion coefficient in action space $D_q(J)$ is obtained in closed form. This expression for $D_q(J)$ is quite general, valid for any choice of

unperturbed Hamiltonian $H_0(J)$. The analysis also shows that the normalized diffusion coefficient does not depend on the beam energy γ_r . The numerical results agree well with the theory.

We evaluate the loss of trapped particles for typical short wavelength FEL parameters. We find that a single frequency sideband with a sideband to carrier power ratio of ≤ 1 can cause half of the particles to detrap over 100 wiggler periods; we have observed total loss of trapped particles for power ratios of ≈ 1 . In cases of wide but discrete sideband spectrum the diffusion length becomes comparable to the wiggler length only at large power ratios (≥ 1). The case of a wide continuous spectrum seems to cause insignificant electron detrapping for the same parameters as above; the typical diffusion length is of the order of 1000 wiggler periods for sideband to carrier power ratios of 1.

In our investigation we have assumed all electromagnetic fields as given. The changes in the particle trajectories are decoupled from the evolution of the fields. At the expense of self-consistency we are able to analyze the situation theoretically and determine the scaling of the diffusion rates on the various FEL parameters. Deterioration in the extraction efficiency has been observed in self-consistent numerical simulations of high power FEL oscillators¹⁰ with high level sideband excitation. The gain per pass in a tapered wiggler is progressively limited as the sideband power goes up and the rate of electron detrapping is accelerated. In an untapered wiggler, on the other hand, particle detrapping is not so important for the main signal efficiency. The total extraction efficiency may actually increase with the sidebands since there are more modes to channel the electron beam energy into.

The remainder of this paper is organized as follows. In Sec. II we construct our analytic model for the study of the stochastic diffusion and discuss the various approximations. To elucidate the analysis we start with a single sideband mode and give a sketchy description of how this can lead to electron detrapping. In Sec. III we examine the structure of the phase space for a monochromatic sideband in detail, using canonical formalism. The threshold for the stochastic transition and the extent of the chaotic regime in phase space are obtained in Sec. IV. In Sec. V the diffusion rate caused by a single sideband mode is examined in connection with the various FEL parameters. In Sec. VI the study is extended to broad (multifrequency) sideband spectra. A distinction is drawn between continuous and discrete spectra. Subsection VI.a covers the case of a broad discrete spectrum and the related diffusion coefficient. Subsection VI.b deals with a broad continuous spectrum and the corresponding quasilinear diffusion coefficient. In Sec. VII the theoretical models are compared with numerical results. The differences in the induced diffusion rates among the three different types of spectra are emphasized. The reduction in the extraction efficiency in a tapered wiggler FEL is computed as a function of the diffusion coefficient. Results and conclusions are summarized in Sec. VIII.

II. GENERAL CONSIDERATIONS

We consider relativistic electrons streaming along the z -direction through the static magnetic wiggler and the radiation fields of the carrier and the sideband. We take all fields to be circularly polarized and of constant amplitude. To simplify the analysis and make the underlying ideas clearer we start out with monochromatic waves for the carrier and the sideband. The total vector potential is then,

$$A(z, t) = \quad (1)$$

$$\frac{1}{2} \left[(e_x - ie_y) A_w e^{i\phi_w} - (e_x + ie_y) A_r e^{i(k_r z - \omega_r t)} - (e_x + ie_y) A_s e^{i(k_s z - \omega_s t)} \right] + cc ,$$

where the subscripts w , r , and s stand for wiggler, carrier and sideband respectively. We assume that all waves propagate with the speed of light c , ignoring the small correction of order ω_p^2/ω_r^2 from the dielectric contribution of the beam. Electrostatic contributions to the fields are neglected for operation in the Compton regime. The phase of the wiggler is given by $\phi_w(z) = \int^z k_w(z') dz'$, where the wave number $k_w(z)$ may change slowly in z on a scale length much longer than the wiggler wavelength $\lambda_w = 2\pi/k_w$. The main signal wave number k_r is doubly Doppler upshifted from the wiggler wavenumber k_w ,

$$k_r = 2\gamma_z^2 k_w , \quad (2)$$

with the upshifting factor $\gamma_z = (1 - \beta_r^2)^{-1/2}$ and $\beta_r = \omega_r/c(k_r + k_w)$.

We have ignored variations in the x - and y -directions. Increased number of dimensions is known to facilitate the transition to chaotic

motion. Therefore, the threshold for stochasticity for variations in the z-direction only will be useful in providing a necessary condition to avoid fast large-scale diffusion. Slow diffusion due to higher dimensionality will in fact persist for the real system below this threshold. As far as particle detrapping is concerned, three dimensional effects are comparatively insignificant, provided that the dependence on x and y is adiabatic. This requires that the frequency of the betatron oscillation, caused by the transverse field gradients¹⁵, be small compared to the electron synchrotron frequency in the ponderomotive bucket.

We have also assumed that the radiation amplitudes remain constant. In case of fast growth rate of the carrier amplitude the particle trajectories are not analytically tractable, even in the absence of sidebands. It is generally expected that the fraction of trapped particles decreases with decreasing carrier amplitude. Therefore the spreading of the radiation beam due to diffraction^{16,17} can also cause detrapping by reducing the carrier amplitude a_r . This detrapping mechanism is independent of the diffusive detrapping caused by sidebands that is examined here.

Normalizing the time t to ω_r^{-1} , the length z to k_r^{-1} , the mass to m_e and the vector potentials according to $a_i = |e|A_i/m_e c^2$ the dimensionless Hamiltonian describing the electron motion in the fields of Eq. (1) is,

$$H = \left[\mu^2 + p_z^2 - 2\lambda a_w a_r \cos(\phi_w + k_r z - \omega_r t) - 2\lambda a_w a_s \cos(\phi_w + k_s z - \omega_s t) \right]^{1/2} \quad (3)$$

$$\mu^2 = 1 + M(a_w^2 + a_r^2 + a_s^2),$$

with $M = 1$ and $\Lambda = 1$. Eq. (3) also describes the fast-time averaged Hamiltonian for a linearly polarized wiggler by setting $M = 1/2$, $\Lambda = [J_0(\zeta) - J_1(\zeta)]/2$ and $\zeta = a_w^2/(4 + 2a_w^2)$.

The terms proportional to $a_w a_r$ and $a_w a_s$ are the ponderomotive potentials due to the combined action of the wiggler with the main signal and the sideband respectively. The resonant velocities for each ponderomotive potential are given by $\beta_i = k_i/(k_i + k_w)$ corresponding to resonant energies,

$$\gamma_i = \left(\frac{\mu^2}{1 - \beta_i^2} \right)^{1/2}, \quad i = r, s. \quad (4)$$

In the vicinity of γ_i the motion of the electrons is determined by the corresponding resonant term inside (3). We may drop the nonresonant term for small radiation amplitudes and linearize (3) for small excursions $\delta\gamma$ around γ_i . From the resulting pendulum equation we find that trapped electrons will undergo oscillations of frequency ω_b around γ_i , forming islands of width $\delta\gamma_i$ in phase space, where ω_b and $\delta\gamma_i$ are given by,

$$\omega_b = \frac{1}{\gamma_i} \left(a_w a_i \mu^2 \right)^{1/2}, \quad \delta\gamma_i = \gamma_i \left(\frac{a_w a_r}{\mu^2} \right)^{1/2}. \quad (5)$$

We call these islands, due to the direct wave-particle resonances, primary islands.

Roughly speaking, irregular motion breaks out as a result of nearby island overlapping¹⁴. The amplitudes a_r , a_s must increase to the point where,

$$\delta\gamma_r + \delta\gamma_s \geq |\gamma_r - \gamma_s|, \quad (6)$$

for an overlapping between the two primary islands to take place. The difference in resonant energies $\Delta\gamma = \gamma_r - \gamma_s$ is given by $\Delta\gamma = \gamma_z \gamma_r^2 \Delta\beta$ where $\Delta\beta = |\beta_s - \beta_r| = (1/2\gamma_z^2) |k_r - k_s|/k_r$. Given that typically $k_s - k_r \sim 2\gamma_z^2 \omega_b$ we find,

$$\Delta\gamma \sim \gamma_r (a_w a_r)^{1/2}. \quad (7)$$

It then follows from (5) to (7) that overlapping and transition to chaotic behavior can take place at $a_s \sim a_r$. This crude estimate demonstrates the potential of chaotic behavior for large amplitude sidebands. The above threshold becomes even smaller in case of a multifrequency sideband spectrum.

We will be interested in evaluating the fraction of the phase space that becomes chaotic as a function of the sideband amplitude. This requires the use of a more refined overlapping criterion. Electrons trapped inside the primary island of the main signal still experience perturbations in their motion caused by the sideband. The perturbation is especially felt by these electrons that have the synchrotron frequency ω_b matching the difference between the frequencies of the main signal and the sideband. This condition defines new secondary resonances between the electrons and the sideband. It is the overlapping among the nearby secondary islands, formed inside the primary island, that determines more accurately the break out and extent of the stochastic behavior.

III. PORTRAIT OF THE PHASE SPACE

The electrons are injected into a FEL with energies near the resonant energy γ_r for the main signal ω_r . Expression (3) can be linearized for small excursions $\delta\gamma/\gamma_r \ll 1$ for electrons not too far from the separatrix. Introducing $\tilde{\gamma} = \gamma - \gamma_r$ and $\psi = (k_w + k_r)z - \omega_r t$ as a new pair of canonical variables and approximating the time $t(z) \approx z/c\beta_r$ we obtain,

$$H(\tilde{\gamma}, \psi; z) = \frac{k_w}{\gamma_r} \tilde{\gamma}^2 + \frac{a_w a_r}{\gamma_r} (\cos \psi + \psi \sin \psi_r) + \frac{a_w a_s}{\gamma_r} \cos(\psi - \delta_s z). \quad (8)$$

In (8) the phase flow is parametrized by the traveled length z inside the wiggler rather than the time t . It was also assumed that the wiggler parameters change slowly compared to the wiggler wavelength $2\pi/k_w$. The term $\sin \psi_r$ parametrizes the rate of change for the resonant energy caused by the change in the wiggler wavelength,

$$\frac{d}{dz} \gamma_r = \frac{k_r a_w a_r}{\gamma_r} \sin \psi_r, \quad (9)$$

where $\psi_r = \pi$ corresponds to an untapered wiggler. The term δ_s in the sideband phase is the Doppler downshifted difference between the signal and the sideband wave numbers,

$$\delta_s = \frac{k_w}{k_r} (k_s - k_r). \quad (10)$$

In the absence of sidebands, $a_s = 0$, the Hamiltonian H_0 is integrable. The unperturbed trajectories in the ponderomotive well are given by $H_0(\tilde{\gamma}, \psi) = K$ where K is the reduced energy in the ponderomotive frame. These orbits take the simplest possible form expressed in terms of the action-angle variables (J, θ) , defined as,

$$J = \frac{1}{2\pi} \oint d\psi \tilde{\gamma}(K, \psi), \quad \theta = \frac{\partial}{\partial J} \int^\psi d\psi' \tilde{\gamma}(K, \psi'), \quad (11)$$

where $K = H_0(J)$ and the path of integration is over the unperturbed orbits. For trapped particles in closed trajectories, the action J is related to the area in phase space enclosed by the orbit. For untrapped particles in open trajectories, the path of integration in Eq. (11) depends on the wiggler type. In case of an untapered wiggler, the orbits are periodic and the limits of ψ integration are from 0 to 2π . In case of a tapered wiggler the path of integration is the segment of the trajectory that begins and ends at $\psi = \psi_s$, enclosing the separatrix. Thus, J remains finite, avoiding an infinite jump in action across the separatrix that would result by considering the full orbit length for unbound orbits¹⁸. J is always periodic in ψ , $J(\tilde{\gamma}, \psi_1) = J(\tilde{\gamma}, \psi_2)$ for $\psi_1 = \psi_2 + 2\pi$, even when H_0 is not (case of tapered wiggler).

Hamiltonian (8) is now transformed under the canonical transformation defined by Eq. (11) into,

$$H(J, \theta; z) = H_0(J) + \frac{a_w a_s}{\gamma_r} \sum_{n=0}^{\infty} Q_n^+(J) \cos(n\theta + \delta_s z) + Q_n^-(J) \cos(n\theta - \delta_s z). \quad (12)$$

$Q_n^+(J)$ are the Fourier coefficients obtained by the decomposition of the perturbing sideband phase $\psi(J, \theta) - \delta_s z$ into harmonics of the angle θ ,

where $\psi(J, \theta)$ is obtained by inverting Eq. (11). In case of constant parameter wiggler J , θ and $Q_n(J)$ are expressed in closed forms given in Appendix A.

$H_0(J)$ is independent of θ so the unperturbed orbits in (J, θ) space are straight lines,

$$J = \text{const.}, \quad \theta = \theta_0 + \kappa_b(J)z.$$

The synchrotron wave number $\kappa_b(J)$ is connected to the bounce length L_b and the synchrotron frequency in the laboratory frame $\omega_b(J)$ with the relation,

$$\kappa_b(J) = \frac{dH_0(J)}{dJ} = \frac{2\pi}{L_b(J)} = \frac{\omega_b(J)}{c\beta_z}. \quad (13)$$

Since $c = 1$ in the normalized units and $\beta_z = 1$ in the cases of interest, we may use $\omega_b(J)$ in place of $\kappa_b(J)$ as well.

Expression (12) for the transformed Hamiltonian reveals the new resonances emerging when a sideband is turned on. Defining the phase of the n th sideband induced harmonic $\theta^{(n)} = n\theta \pm \delta_s z$, the stationary phase condition reads,

$$\pm n\kappa_b(J) - \delta_s = 0, \quad \text{or} \quad \pm n\beta_z\omega_b(J) - \delta_s = 0. \quad (14)$$

Thus, particles, originally in unperturbed orbits $J = J_n$, resonate with the sideband when the n th harmonic of their synchrotron period $\omega_b(J_n)$ matches the downshifted frequency difference between the sideband and the carrier signal.

For a given n and sufficiently small a_s we may keep only the resonant term $\theta^{(n)}$ to examine the motion in the vicinity of J_n . This is formally achieved by the canonical transformation,

$$\begin{aligned}\theta &= n\theta - \delta_s z, & I &= \frac{1}{n} J, \\ Z &= \delta_s z, & I_Z &= \frac{1}{\delta_s} K + \frac{1}{n} J,\end{aligned}\tag{15}$$

coming from the generating function $F(\theta, z, I, I_Z) = (n\theta - z)I - zI_Z$. The resulting Hamiltonian is,

$$H_n(I, I_Z, \theta, Z) = H_0(nI) + \delta_s(I_Z - I) + \frac{a_w a_s}{\gamma_r} Q_n(nI) \cos\theta + O(a_s^2).\tag{16}$$

The fixed points (J_n, θ_n) are found from,

$$\frac{d\theta}{dZ} = \frac{\partial H_n}{\partial I} = \frac{\partial H_0}{\partial I} - \delta_s = 0,\tag{17a}$$

$$\frac{dI}{dZ} = -\frac{\partial H_n}{\partial \theta} = \frac{a_w a_s}{\gamma_r} Q_n(nI) \sin\theta = 0.\tag{17b}$$

Using relations (15) for the transformed variables we recover from (17a) the resonant condition (14) while (17b) indicates $\theta_n = k\pi / n$, $k = 0, 1, \dots, n-1$.

In short, a single frequency sideband causes chains of secondary islands to appear inside the original primary island. Each chain corresponds to a given harmonic n and is centered around the stable fixed points J_n, θ_n . The structure of the phase space is shown in Figs. 1 and 2. They are surfaces of section, created by numerically

integrating the original equations of motion from Hamiltonian Eq. (8) and then recording the intersection point of each trajectory with the plane $z = 2\pi/\delta_s$. The $\tilde{\gamma}$ vs. ψ plots are on the left side in Figs. 1 and 2. The plots on the right side show the same surfaces of section in action-angle variables, produced by the transformations (11). The bounce frequency around a given secondary island is found by linearly expanding the resonant Hamiltonian (16) in $\delta I = I - I_n$. From the resulting pendulum equation and from relations (15) one finds that the secondary synchrotron period Q_n near the center is given by,

$$Q_n = n \left[\left(\frac{d\omega_b}{dJ} \right)_{J_n} \frac{a_w a_s}{\gamma_r} Q_n^{\pm}(J) \right]^{1/2}, \quad (18a)$$

while the half-width of the island δJ_n is

$$\delta J_n = \left[2 \frac{a_w a_s}{\gamma} \frac{Q_n(J_n)}{(d\omega_b/dJ)_{J_n}} \right]^{1/2}. \quad (18b)$$

Representation (12) for the Hamiltonian (8) is formally independent on the details of the transformations (11). Consequently, the same stability analysis applies for constant as well as variable parameter wigglers.

IV. THRESHOLD FOR ERRATIC MOTION

When the sideband amplitude exceeds a certain amplitude α_s regarded as the stochasticity threshold, the presence of even one sideband frequency suffices to transform the regular coherent motion, such as in Fig. 1, to the irregular unbounded motion shown in Fig. 2. The mechanism for this radical change in behavior can be briefly described as follows. The trajectories emanating from the unstable fixed points (X-points) of a secondary island do not actually join smoothly around that island. They intersect infinite times with each other^{12,13} due to the effect of the other harmonics $n' \neq n$ that were ignored during the local approximation Eq. (16). A thin layer of fuzzy motion thus surrounds each island chain of given n . As the amplitude a_s increases, the width of each island increases according to (18b) and so does the thickness of the stochastic layer around that island. At a given point the stochastic layers around the two neighboring island chains n and $n+1$ overlap¹⁴, allowing particles to hop from one island to another. This signifies the beginning of unbounded, random motion in J characterized as stochastic diffusion.

Various methods of different accuracy have been developed for estimating the stochasticity threshold^{12,14}. An approximate criterion that works well in most cases is,

$$\delta J_n + \delta J_{n+1} \geq \frac{2}{3} \Delta J_n, \quad (19)$$

where δJ_n , δJ_{n+1} are the separatrix half-widths and $\Delta J_n = J_{n+1} - J_n$ is the distance between the separatrix centers for the n and $n+1$ harmonics respectively. For small widths δJ and distances ΔJ compared to J we may expand

$$\omega_b(J_{n+1}) - \omega_b(J_n) = \left(\frac{\partial \omega_b}{\partial J} \right)_{J_n} \Delta J_n \approx \frac{\omega_b(J_n)}{n}, \quad (20)$$

and use (18b) with $J_{n+1} \approx J_n$ to obtain the amplitude $a_s(n)$ for overlapping

$$a_s(n) \approx \left(\frac{2}{3n} \right)^2 \frac{\omega_b(J_n)}{(d\omega_b/dJ)_{J_n}} \left(\frac{\gamma_r}{2a_w Q_n(J_n)} \right). \quad (21)$$

The outermost islands centered at $J_n \approx J_s$, correspond to larger shear $d\omega_b(J)/dJ$, smaller $\omega_b(J)$ and higher harmonics n , for given $\omega_s - \omega_r$. According to (21) the threshold $a_s(n)$ is lower near the separatrix and the outermost secondary islands will be the first to overlap. The overlapping is progressively extending to smaller J_n and lower n as a_s increases. The macroscopic stochastic layer first appears near the original separatrix of the primary island and spreads to the interior of the trapped particle bucket. We take the amplitude when the two innermost harmonics overlap as the threshold for "global" stochastic transition, $\alpha_s \equiv a_s(n_1)$. The lowest possible harmonic n_1 for given frequency ω_s is defined by the resonant condition (14). For J_n small we have both δJ and ΔJ of order J and the approximations that led to (21) are not valid. In this case, the exact expressions for J and $\omega_b(J)$ must be applied inside the criterion (19).

We may obtain the dependence of $a_s(n)$ on the various parameters using Eqs. (A4) and (A7), setting $d/dJ = (d\lambda/dJ) d/d\lambda$ and utilizing the properties of the elliptic integrals to compute the derivatives in Eq. (21). We find that,

$$\frac{a_s(n)}{a_r} \approx \frac{1}{n^2} F^2(\lambda_n) , \quad (22)$$

where

$$F(\lambda_n) = \left\{ \frac{E_1(\lambda_n) \lambda_n^2 (\lambda_n^2 - 1)}{E_2(\lambda_n) - (1 - \lambda_n^2) E_1(\lambda_n)} \right\}^{1/2} \left(2Q_n(\lambda_n) \right)^{-1/2} .$$

The threshold for extensive stochasticity $\alpha_s \equiv a_s(n_1)$ is independent of γ and a_w . The trapping parameter λ_n is determined uniquely from J_n according to $\lambda_n = H_0(J_n) \gamma_r / a_w a_r + 1/2$ (see Appendix A). Thus, the sideband frequency ω_s , related to $\omega_b(J_n)$ through the resonant condition (14), is the only parameter that α_s/a_r depends on. The scaling in (22) is still valid in case of large secondary island width with a modification in the numerical factor F .

In Fig. 3a we plot in solid line the threshold α_s for extensive stochasticity, when the two innermost secondary island chains overlap, as a function of the frequency difference $\omega_c - \omega_r$. The dotted line shows the threshold for overlapping between the next two secondary island chains. Some deeply trapped orbits, near the center of the original primary island, still persist when a_s is close to α_s . The extent of the area unaffected by the irregular motion when $a_s \approx \alpha_s$ is given approximately by $J < J_c$ where $J_c \approx J_n - \delta J_n$. In Fig. 3b we plot the portion J_c/J_s of the remaining "good" trajectories when the sideband amplitude equals α_s as a function of $\omega_s - \omega_r$. It is seen that the threshold α_s is larger and the extent of the stochastic regime is maximized as well for frequency mismatch near a harmonic of the synchrotron frequency $\omega_b(0)$ at the bottom of the ponderomotive well.

The threshold α_s for overlapping is considerably lower but the extent of the stochastic regime also diminishes for frequencies far from a harmonic of the central synchrotron frequency.

A typical phase portrait for a sideband amplitude a_s slightly above α_s is shown in Fig. 2b. Two different kinds of regions coexist: a stochastic regime where diffusive behavior prevails, interrupted here and there by islands of regular motion, remnants of the original regular motion. The stochastic regimes are interconnected allowing unbounded particle transport. The rate of diffusion as well as the decorrelation times are not uniform in phase space but depend on both J and θ .

When a_s is increased well above α_s the chaotic motion engulfs almost 100% of the phase space (Fig. 2c). The decorrelation time is short everywhere in phase space. In this parameter regime the behavior of the system can be described by a diffusion coefficient $D(J)$ depending on the action J only and insensitive to the frequency of the driving sideband. Total stochastization of the island interior occurs roughly when the sideband amplitude grows to the point where the stable fixed point $\tilde{\gamma} = 0$, $\psi = \pi + \psi_r$ at the center of the original island becomes unstable.

V. NARROW FREQUENCY BAND DIFFUSION

We will examine first the diffusion caused by the presence of one single frequency, large amplitude sideband. This is a relevant approximation in case of a narrow sideband spectrum. The term narrow implies a spectral width $D\omega_s$ much smaller than the frequency separation $\omega_s - \omega_r$, typically of the order $2\gamma_z^2 \omega_b$. We examine the evolution of a monoenergetic distribution $f(J; z=0) = \delta(J - J_0)$ by numerically integrating the equations of motion. We plot $\langle \Delta J^2 \rangle$, $\langle J \rangle$ and $2 \langle \Delta J^2 \rangle / z$ against the distance z in Figs. 4a, 4b, and 4c respectively. The electrons are initially uniformly distributed in θ with constant action $J_0 = 0.7 J_s$. Different curves in the same frame correspond to different sideband amplitudes a_s at a given frequency ω_s .

For a constant diffusion coefficient D , independent of J , the average $\langle J \rangle$ and the mean square deviation $\langle \Delta J^2 \rangle = \langle J^2 \rangle - \langle J \rangle^2$ would evolve as $\langle \Delta J^2 \rangle = (1/2) D z$, $\langle J \rangle = J_0$. The dashed curves in Figs. 4a - 4c correspond to a sideband amplitude a_s below the stochasticity threshold α_s . The deviation $\langle \Delta J^2 \rangle$ asymptotes to a constant after an initial increase while the ratio $\langle \Delta J^2 \rangle / z$ tends to zero for large z . In this case stochasticity is localized. Different stochastic regimes are still separated by "good" integrable orbits (KAM surfaces) located in between. Electrons diffuse until they are stopped at the boundaries of the stochastic regimes that "compartmentalize" the phase space. The solid curves in Figs. 4a - 4c correspond to sideband amplitude above the global stochasticity threshold α_s . This means that the last good orbit has been destroyed allowing different stochastic regimes to interconnect. $\langle \Delta J^2 \rangle$ now increases monotonically and the ratio $\langle \Delta J^2 \rangle / z$ remains finite for large z . The fact that the diffusion rate is not

constant, and that the average $\langle J \rangle$ changes away from the initial value J_0 , shows that D depends strongly on J .

In principle, one could determine a local $D(J)$ by advancing test distributions $\delta(J-J_0)$ of various J_0 over short distances z . Then the Fokker-Planck equation for any initial distribution $f_0(J)$ could be solved numerically using $D(J)$. Here, instead, we elect to measure directly the effective diffusion rate associated with a given type of initial distribution. We do so by integrating numerically the equations of motion, Hamiltonian (8), for a number of particles (typically 400) assuming constant amplitude for the electromagnetic fields. A uniform initial distribution in phase space with trapped particles inside the (unperturbed) separatrix is chosen, $f_0(J) = [1 - S(J - J_s)]/J_s$ where S is the step function. This situation is relevant with the operation of tapered wiggler FELs where the trapped particles in the ponderomotive bucket are decelerating, falling quickly behind the untrapped particles and thus creating large distribution gradients near the separatrix.

The two questions of practical interest are (a) what percentage of the particles will eventually get detrapped and (b) how fast do they leak outside the separatrix. For our uniform initial distribution the maximum fraction of particles becoming detrapped equals the fraction of the inside of the separatrix area that becomes chaotic. In Fig. 5a we plot the fraction f_d of the particles that cross the original separatrix J_s as a function of the traveled wiggler length for values of $q = a_s/a_r$ below the threshold for extended stochasticity. In all cases an initial stage of quick diffusion is followed by a long period where the average number of untrapped particles remains practically constant. The results are consistent with the existence of a boundary in phase space (KAM surface) separating two regimes: the one of unbounded, chaotic motion

from the one filled with regular, coherent orbits of particles that remain trapped. Only electrons in the area between the last integrable surface and the old unperturbed separatrix will diffuse until that area is depleted. A fraction $1 - f_d$ of the original primary island area will remain trapped for an arbitrarily long time, as long as a_s remains below the threshold α_s associated with the particular sideband frequency. This fraction is shrinking as a_s increases and the bucket "peels off". The situation when a_s exceeds α_s is shown in Fig. 5b. The fraction of untrapped particles f_d reaches 1 in all cases, meaning complete absence of particle confinement in the bucket. All particles can eventually escape with a rate that increases with increasing a_s .

Numerical results showing the fraction of detrapped particles f_d after 100 wiggler periods as a function of a_s/a_r are plotted in Fig. 6 for various sideband frequencies $|\omega_s - \omega_r|$. The length over which approximately half of the initially trapped particles get detrapped will be discussed in the next section, in comparison with the diffusion rates from other types of sideband spectra.

VI. BROAD FREQUENCY BAND DIFFUSION

So far stochastic electron detrapping caused by a single frequency sideband has been examined. It was argued that when the excited sideband spectrum is narrow enough, i.e., $D\omega_s \ll 2\gamma_z^2 \omega_b$, the situation can be reasonably approximated by a single frequency sideband. Here, we consider the situation when a broad spectrum of frequencies have been excited, $D\omega_s \geq 2\gamma_z^2 \omega_b$. We will make a distinction between a continuous and a discrete spectrum. In case of a discrete spectrum the distance between two nearby sideband frequencies is much larger than the width of an individual spectral line. In the opposite case, when various peaks in the spectrum merge together, we will talk about a continuous spectrum. We may model numerically both cases by introducing a modulation in the sideband phase of Hamiltonian Eq. (11),

$$H(\gamma, \psi; z) = \frac{k_w}{\gamma_r} \gamma^2 + \frac{a_w a_r}{\gamma_r} (\cos \psi + \psi \sin \psi_r) + \frac{a_w a_s}{\gamma_r} \cos(\psi + A \sin v z - \delta_s z), \quad (23)$$

that is transformed in action-angle variables as

$$H(J, \theta; z) = H_0(J) + H_1(J, \theta; z),$$

$$H_1(J, \theta; z) = \quad (24)$$

$$\frac{a_w a_s}{\gamma_r} \sum_{m=-\infty}^{\infty} J_m(A) \sum_{n=0}^{\infty} Q_n^+(J) \cos[n\theta + \delta_s(m)z] + Q_n^-(J) \cos[n\theta - \delta_s(m)z].$$

The frequency mismatch values $\delta_s(m)$ and the corresponding sideband frequencies $\omega_s(m)$ are given by,

$$\delta_s(m) = \delta_0 + m \nu, \quad \omega_s(m) = \omega_{s0} + 2 m \gamma_z^2 \nu, \quad (25)$$

where $\omega_{s0} = \omega_r + 2\gamma_z^2 \delta_0$. Since the Bessel function coefficients become vanishingly small, $J_m(A) \ll 1$ for $A \gg m$, the width of the spectrum is given by $D\delta_s \sim A \nu$ or $D\omega_s \approx 2\gamma_z^2 A\nu$.

In order to examine the connection between diffusion rates and the types of the sideband spectra, we divide the latter into three general categories: narrow, broad discrete and broad continuous. The passage from one regime to the other is not gradual but characterized by abrupt changes in the diffusion coefficients. Thus, from the diffusion point of view, the distinction among the spectral types is not arbitrary but based on certain relations between the parameters A and ν . In all three regimes of the parameter space the rate of diffusion is proportional to the ratio of the total sideband power to the carrier power. The scaling of the coefficients of this proportionality on the various FEL parameters, however, differs from one regime to the other.

Both cases of the broad spectrum are characterized by a width $D\omega_s$ in the excited frequencies that is larger than the upshifted synchrotron frequency ω_b ,

$$D\omega_s > 2 \gamma_z^2 \omega_b, \quad \text{equivalent to} \quad \nu > \frac{\omega_b}{A}, \quad (26)$$

with $A \gg 1$. The further distinction between discrete or continuous spectrum is related to the separation between nearby frequencies. We find that when $\omega_b/A^{1/2} > \nu > \omega_b/A$ the diffusion rate agrees well with the quasilinear diffusion coefficient. A different coefficient is derived for the case when $\nu > \omega_b/A^{1/2} > \omega_b/A$, in agreement with the numerical simulations. Consequently the separation $\omega_b/A^{1/2}$ between

nearby modes marks the transition from a discrete to a continuous type of behavior. Departure from the quasilinear diffusion coefficient has also been observed numerically in previous literature¹⁹ when the frequency separation between nearby modes was not "small enough". Here a condition for the discrete-to-continuous transition has been obtained.

For any spectral type, the sideband amplitude must be above the stochastisity threshold in order to trigger electron diffusion. Using the same method of nearby resonance overlapping as in Sec. III, and the Hamiltonian Eq. (25) we find that the threshold in case of a multifrequency spectrum is given by,

$$\tilde{\alpha}_s \approx \frac{\nu}{\omega_b J_m(A)} \alpha_s, \quad (27)$$

where α_s is the threshold for the single sideband frequency. Thus $\tilde{\alpha}_s$ decreases with decreasing frequency separation ν . Condition (27) guarantees the stochastization of the particle orbits. The frequency separation among sidebands must be limited by the additional condition $\nu < \omega_b/A^{1/2}$, as stated in the previous paragraph, if one wishes to simulate quasilinear diffusion with a discrete spectrum.

A. Broad Discrete Spectrum.

We now evaluate the diffusion coefficient for a broad, discrete spectrum. The equation of motion for J can be written as,

$$\frac{dJ}{dz} = - \frac{\partial H_1}{\partial \theta} = - \frac{\partial H_1}{\partial \psi} \frac{d\psi}{d\theta} = \Lambda \frac{a_w a_s}{\gamma_r} \sin \left(\psi + A \sin \nu z - \delta_s z \right) |V(\psi_{mx}) - V(\psi)|^{1/2},$$

using Eq. (A2) for $d\psi/d\theta$. Due to the presence of many frequencies in the spectrum $J(z)$ executes a complicated oscillatory motion with the average $\langle J \rangle$ changing very little most of the time. J however receives a large kick ΔJ near resonances, where the phase $\Phi = \psi + A \sin \nu z - \delta_s z$ of the multifrequency perturbation H_1 varies slowly. The resonant condition is,

$$\frac{d\Phi}{dz} = \frac{k_w \tilde{\gamma}}{\gamma_r} + A \nu \sin \nu z - \delta_s = 0, \quad (28)$$

at some $z = z_i$. Given that $k_w \tilde{\gamma} / \gamma_r \leq \omega_b$, collective effects due to many frequencies are important for the resonance in Eq. (28) when $A \nu > \omega_b$. On this basis inequality (27) signifies the transition from a narrow to a broad spectrum. Let us consider the case $A \nu \gg \omega_b$. Then the resonances occur at $z_i \approx i\pi/\nu$, i integer, and the interval between successive resonances is $\Delta z \approx \pi/\nu$. Expanding the phase $\Phi(z)$ in the equation of motion for J around the resonance z_i ,

$$\Phi(z) \approx \Phi_i + \frac{1}{2} \left[\omega_b^2 (\sin \psi_i + \sin \psi_r) + A \nu^2 \cos \nu z_i \right] (z - z_i)^2, \quad (29)$$

and extending the limits of integration to $z = \pm \infty$ we obtain,

$$DJ_i \approx \frac{a_w a_r}{\gamma_r} \left(\frac{2\pi}{\omega_b^2} \right)^{1/2} \frac{\cos \left(\Phi_i \pm \frac{\pi}{4} \right) |V(\psi_{mx}) - V(\psi_i)|^{1/2}}{\left((\sin \psi_i + \sin \psi_r) + A \left(\frac{\nu}{\omega_b} \right)^2 \right)^{1/2}}, \quad (30)$$

where $\psi_{mx}(J)$ is the turning point for an unperturbed trajectory of given J . When $A \nu^2 \gg \omega_b^2$ both Δz and ΔJ depend on the features ν and A of the sideband spectrum and not on the bounce frequency ω_b . We classify the cases with frequency separation $\nu > \omega_b / A^{1/2}$ as broad discrete spectra. They obey a distinct scaling in the diffusion coefficient that will be

derived below. We find the cases with $v < \omega_b/A^{1/2}$ to agree numerically with the quasilinear diffusion that will be studied in the next subsection.

The resonant phases ϕ_i between two successive jumps of ΔJ become quickly decorrelated when a_s grows above the stochastisity threshold. Because the relation between ϕ_i and ψ_i involves the distance z_i , ϕ_i and ψ_i will also become decorrelated, $\langle \cos \phi_i \cos \psi_i \rangle = 0$. Assuming complete decorrelation between two successive jumps we obtain,

$$D_v = \frac{2 \langle \Delta J_i^2 \rangle}{Dz} = \frac{2 a_w^2 a_r^2}{\gamma_r^2 A v} \langle |V(\psi_{mx}) - V(\psi_i)| \rangle, \quad (31)$$

where the angular brackets $\langle \dots \rangle$ signify the average over ψ_i for constant J . For practical purposes it is more convenient to rescale the diffusion coefficient so that the distance $\underline{z} = z/\lambda_w$ is measured in terms of wiggler wavelengths and the action $\underline{J} = J/J_s$ signifies the location relative to the separatrix. In these units, using Eq. (A4) for J_s and setting $v / \omega_b(0) = r$ we obtain,

$$D_v = \frac{2\pi}{k_w} \frac{D_v}{J_s^2} \sim \frac{\pi^3}{8} \frac{g^2 \zeta}{A r} \left(\frac{a_w a_r}{1 + a_w^2} \right)^{1/2} \frac{a_s^2}{a_r^2}. \quad (32)$$

The term g is a scaling factor, the ratio of the separatrix area for an untapered wiggler to that of a tapered wiggler, $g = J_s(\psi_r=\pi)/J(\psi_r)$, and depends only on ψ_r^1 . The term $\zeta \sim 1$, coming from the averaging over ψ_i in Eq. (31), is computed in Appendix B. The typical diffusion length L_d , the traveled distance inside the wiggler over which the average trapped particle crosses the separatrix, is estimated from the diffusion Eq.

(22) by taking $\langle \Delta J^2 \rangle = J_s^2$, $L_d \sim J_s^2 / D_w$. Thus, the diffusion length in wiggler periods $N_d = L_d / \lambda_w$ is the inverse of D_w ,

$$N_d \sim \frac{1}{D_w}. \quad (33)$$

B. Broad Continuous Spectrum

Next we consider the case of a sideband wave package,

$$a_s(z, t) = \frac{1}{2\pi} \int dk_s a_s(k_s) e^{ik_s z - i\omega(k_s)t}, \quad (34)$$

of finite spectral width Dk_s centered around k_{s0} . Our purpose is to obtain the diffusion coefficient for a continuous spectrum using the methods of the quasilinear theory. Upon using expression (34) for the fields, the Hamiltonian representation in action-angle variables assumes the form,

$$H(J, \theta; z) = H_0(J) + \frac{a_w}{\gamma_r} \sum_{n=0}^{\infty} Q_n^{\pm}(J) \int dk_s a_s(k_s) \cos [n\theta \pm \delta(k_s)z], \quad (35)$$

where $\delta(k_s)$ is given by,

$$\delta(k_s) = \delta_{s0} + (k_s - k_{s0}) \frac{k_w}{k_r} + \left(\frac{v(k_s) - v(k_r)}{c} \right) k_{s0}, \quad (36)$$

and $\delta_{s0} = (k_w/k_r)(k_{s0} - k_r)$ in the spirit of Eq. (10). The last parenthesis in the right-hand side of (36) is of order $(\omega_p/\omega_r)^2$ resulting from the dispersive effects in the sideband spectrum. The

finite k_w provides phase slippage among the ponderomotive phases of various wavenumbers k_s , a necessary condition for the validity of the quasilinear theory, even when the dispersive effects of the last term in (36) are negligible, i.e., $\gamma_z^2 (\omega_p/\omega_r)^2 \ll Dk_s/k_s$.

The resonant condition between a sideband wavelength k_s and a given harmonic n now reads $\pm n\omega_b(J_n) = \delta(k_s)$. For each harmonic n there exists a wide band of resonant orbits centered around J_{no} and of width DJ_n defined by,

$$DJ_n = (d\Omega_b/dJ)_{J_{no}}^{-1} (k_w/k_r) Dk_s, \quad \pm n\omega_b(J_{no}) = \delta_{so}. \quad (37)$$

One condition for the applicability of the quasilinear theory is that the phase mixing due to Dk_s occurs much faster than the bounce period around a secondary island in phase space. In this way, electrons, that otherwise would execute periodic orbits around some fixed point, lose coherence sufficiently fast to allow random motion of the Fokker-Planck type. Taking the decorrelation length for the phase $l_d \sim 2\pi/D\delta(k_s)$ and applying Eq. (18a) for the bounce period around the n th harmonic we obtain

$$\frac{Dk_s}{k_s} \gg \frac{n}{2} \left(\frac{\pi Q_n^{\pm}}{\sqrt{2}} \right)^{1/2} \left(\frac{\lambda a_w a_r}{1 + a_w^2} \right)^{1/2}. \quad (38)$$

Inequality (38) guarantees the diffusive behavior within the band DJ_n around J_{no} given by (37). Large scale diffusion, permitting transport of deeply trapped particles across the separatrix J_s of the original primary island, requires that different stochastic bands touch each other, $DJ_n + DJ_{n+1} \geq \Delta J_n$, or, using a similar approach as in Eqs. (19) and (20),

$$\frac{Dk_s}{k_s} > \frac{1}{8n} \left(\frac{\pi Q_n^{\pm}}{\sqrt{2}} \right)^{1/2} \left(\frac{\Lambda a_w a_r}{1 + a_w^2} \right)^{1/2}. \quad (39)$$

The right-hand sides of Eqs. (38) and (39) are of the same order as the upshifted synchrotron period for the main bucket. Thus both conditions are satisfied when,

$$\frac{Dk_s}{k_s} \gg 2 \gamma_z^2 \frac{\kappa_b(0)}{k_r}. \quad (40)$$

Note that (40) is the same as the condition (26) that defines the wide spectrum, obtained in the previous subsection using different arguments. Then the evolution of the initial distribution $f_0(J)$ is globally described by a diffusion equation,

$$\frac{\partial f}{\partial z} = \frac{\partial}{\partial J} D_q(J) \frac{\partial f}{\partial J}. \quad (41)$$

Applying the standard procedures of the quasilinear theory^{20,21} (see appendix C) and taking the limit of small growth rate for the sidebands, $\text{Im}(k_s)/k_s \ll 1$, we obtain,

$$D_q(J) = \frac{k_r}{4} \frac{k_r}{k_w} \frac{a_w^2}{\gamma_r^2} \sum_{n=0}^{\infty} n^2 |Q_n^{\pm}(J)|^2 \int dk_s W_s(k_s) \delta(k_s - k_n), \quad (42)$$

$$k_n = k_r \pm \frac{k_r}{k_w} n \kappa_b(J).$$

According to the condition (40) for the validity of the quasilinear

theory, the wave package has a wide spectrum $Dk_s \sim N(k_r/k_w)\omega_b(0)$ with N large. The wave components $a_s(k_n)$ fall off slowly for $n < N$ while the Fourier coefficients $Q_n(J)$ decay rapidly with n . Then we may factor out the average spectral power density $W_s = (1/Dk_s) \int dk_s W_s(k_s) \approx a_s^2/Dk_s$ in Eq. (34) getting,

$$D_q(J) \approx \frac{k_r}{4} \frac{k_r}{k_w} \frac{a_w^2}{\gamma_r^2} W_s \sum_{n=0}^{\infty} n^2 |Q_n^{\pm}(J)|^2. \quad (43)$$

The infinite sum in the right-hand side of (43) is computed in Appendix C. The summation technique does not require the knowledge of the individual coefficients $Q_n(J)$ and the result depends only on the quantities J and $\omega_b(J)$ for the unperturbed Hamiltonian $H_0(J)$. We then obtain the diffusion coefficient in closed form,

$$D_q(J) = \frac{k_r a_w^2 \gamma_z^2 W_s k_w J}{\gamma_r^3 \omega_b(J)}. \quad (44)$$

We note in passing that the method used to obtain expression (44) for $D_q(J)$ is quite general and valid for any integrable dynamical system $H_0(J)$ that is subject to an external perturbation. In particular, it should be applicable to a variety of RF heating methods in fusion plasmas, commonly involving a strong, narrow-band pump wave embedded in a wide, parametrically excited, fluctuation spectrum.

Using the expressions (A3) and (A7) for the action J and the synchrotron frequency $\omega_b(J)$ we find that the diffusion coefficient goes to zero at the centre of the primary island $J = 0$, has a logarithmic singularity at the separatrix $J = J_s$ and falls off away from it. In

normalized units, with the wiggler wavelength λ_w as the unit length and the action J_s at the separatrix as the unit action, we have,

$$D_{-q}(J) = \frac{2\pi}{k_w} \frac{D_q(J)}{J_s^2} . \quad (45)$$

Choosing the value $J = J_s/2$ inside $D_q(J)$ we obtain an estimate for the effective diffusion coefficient associated with the uniformly filled distribution,

$$D_{-q} \sim \frac{\pi}{4} \frac{g a_w a_r}{\Lambda (1+a_w^2)} \frac{a_s^2}{Dk_s a_r^2} , \quad (46)$$

where g is the same scaling factor as in Eq. (32).

Note that both expressions (32) and (46), corresponding to the two different spectral types, are independent of γ_r . Thus, for the same wiggler parameters and total sideband power, the detrapping distance in wiggler periods is independent of the electron beam energy. The dependence of the effective diffusion rate on the wiggler tapering enters through the form factor $g(\psi_r) = J_s(\pi)/J(\psi_r)$. As the rate of tapering increases and ψ_r shifts further from π , g increases¹ and accelerates the effective diffusion rate. This happens because the trapped area in phase space, parametrized by J_s , is shrinking as the tapering progresses, while the sideband induced excursions remain the same, depending mainly on the sideband strength and spectrum. This

shortens the average detrapping time for a particle. The diffusion by broad discrete spectrum, Eq. (32) scales as g^2 , while the quasilinear diffusion, Eq. (46), scales as g . Thus the former is affected more by tapering than the latter.

VII. NUMERICAL RESULTS

The numerically computed diffusion coefficient \underline{D} and the diffusion length in wiggler periods $N_d = 1/\underline{D}$ are plotted against the sideband to carrier power ratio $P = \sum_n a_s^2(\omega_n)/a_r^2 = W_s/W_r$ in Figs. 7 and 8 respectively for the three different types of spectra. We have integrated numerically the equations of motion for 400 particles of a uniform initial distribution inside the bucket. The field intensities remained constant at $a_r = 5 \times 10^{-5}$, $a_w = 2$ and $\gamma_r = 25$. All the numerical results in this paper correspond to a tapered wiggler with $\psi_r = 7\pi/6$. A clear separation in the diffusion rates is observed among the various spectral types. The narrow frequency results (triangles) were obtained using the Hamiltonian (8) with a single sideband frequency $\omega_s/\omega_r = 1.016$. The results for a broad discrete spectrum (circles) were obtained using (23) with $A = 20$, $\omega_s/\omega_r = 1.016$ and $\nu = 0.5 \delta_s$. The continuous spectrum (squares) was modeled by $A = 100$, $\nu = 0.05 \delta_s$. The solid lines, corresponding to the theoretical results of Eqs. (32) and (46), are in good agreement with the numerics. Theoretical predictions for the single frequency case were not made. We stress, however, the difference between single frequency results and quasilinear theory in this case. The agreement that has been observed in some other cases²² is not generic but particular to certain systems.

Figure 9 illustrates the difference of the electron response to different sideband spectra. The plots on the left side are typical orbits $J(z)$ for selected particles along the wiggler. The trajectories in all plots are generated by the same initial conditions for the electrons and the same FEL parameters a_w , a_r and k_w , as well as the same mean square sideband power $\langle a_s^2 \rangle$. The spectral parameters A and ν ,

however, are different so that each of the figures (a) to (c) corresponds to one of the three spectral types defined earlier. The dashed line marks the position of the unperturbed separatrix J_s . The corresponding distribution functions $f(J, z)$ at the beginning, $z = 0$, halfway inside, $z = 50\lambda_w$, and at the end, $z = 100\lambda_w$ of the wiggler are plotted in the right-hand side of Figs. 9a-9c respectively.

In Fig. 10 we plot the diffusion coefficient for a uniformly filled bucket as a function of the energy γ_r , fixing the wiggler parameters. It is clear that the diffusion rate (measured again in number of wiggler periods) is independent of the beam energy, provided the synchrotron frequency ω_b stays in the same parameter regime.

Once the diffusion coefficients are known, some estimate can be made of the related reduction in efficiency over the wiggler length. The number of trapped particles at any point z is given by

$n_b = \int_0^S dJ f(J, z)$. Using the diffusion Eq. (41) with $D(J=0) = 0$ one obtains the rate of change in the number of trapped particles,

$$\frac{dn_b}{dz} = n_b(z) D(J_s) \frac{\partial f(J_s, z)}{\partial z}. \quad (47)$$

The leakage rate for trapped particles changes along z as the slope of the distribution $f(J, z)$ changes. To estimate the average leakage rate we assume that $f(J, z)$ remains Gaussian in J with an average width equal to the separatrix action J_s . We estimate from (47) the e-folding length $L_d = -n_b^{-1}(dn_b/dz)$ for the number n_b of trapped particles,

$$L_d = D(J_s) J_s^{-2}. \quad (48)$$

Assuming that $n_b(z) = n_b(0) \exp(-z/L_d)$, the number of detrapped particles between z and $z + \Delta z$ is $\Delta n(z) = n_b(0)L_d^{-1} \exp(-z/L_d) \Delta z$. These particles gave up an amount of energy $\Delta E(z) = [\gamma_r(0) - \gamma_r(z)] \Delta n(z)$ as radiation. Integrating $\Delta E(z)$ over the wiggler length for a linearly tapered wiggler $\gamma_r(z) = \gamma_r(0) - z\Delta\gamma/L_w$, we find the total energy extracted from the particles that were detrapped at some point inside the wiggler. Adding the contribution $[\gamma_r(0) - \gamma_r(L_w)] n_b(L_w)$ from the particles that remained trapped throughout the wiggler length, we come up with,

$$\eta = \eta_0 \frac{L_d}{L_w} \left(1 - \exp \left(-\frac{L_w}{L_d} \right) \right), \quad (49)$$

where $\eta_0 = \Delta\gamma/\gamma_r(0)$ is the efficiency without induced diffusion. The loss of amplification will, in general, be distributed among all the radiation modes and (49) reflects the total power loss in all frequencies. The extraction efficiency η for a linearly tapered wiggler is plotted in Fig. 11 versus the sideband to carrier power ratio P , obtaining the corresponding value for L_d/L_w from the results in Fig. 8.

VIII. CONCLUSION

The diffusion in phase space caused by sideband excitation during FEL operation was studied. It was shown that the characteristic rates for this process depend on the structure of the sideband spectrum, falling into one of the following general categories: narrow, wide discrete or wide continuous spectrum. In all cases, the diffusion coefficient was found proportional to the ratio of the total power in the sidebands to the power in the main FEL signal $D \propto C W_s/W_r$. The coefficient C , however, is connected to the spectral type under consideration. From Eqs. (32) and (46) we see that, apart from numerical factors of order unity, C scales as $(a_w a_r)^l$ with $l = 1/2$ for a discrete and $l = 1$ for a continuous spectrum. Therefore, given the typical FEL values of $a_w \leq 10$ and $a_r \leq 10^{-3}$ an order of magnitude reduction in diffusion occurs in the transition from a discrete to a continuous sideband spectrum. It was also observed numerically that the highest diffusion rate occurs when all the sideband power is in a single frequency. In this case, however, a portion of the particles will remain trapped for arbitrary long wigglers if the sideband amplitude is below the threshold for extensive stochasticity. The stochasticity threshold is progressively reduced as the sideband power is distributed into an increasing number of frequencies. Yet the rate of diffusion also slows down with increasing spectral width and decreasing mode separation. Thus, the minimum reduction in the FEL energy extraction efficiency will occur for continuous sideband spectra. Although control of the sideband structure does not seem plausible, experiments show that a wide spectrum is naturally excited during FEL operation. This would allow enough power build-up before serious deterioration in efficiency, due to detrapping,

to occur. The diffusion length, measured in wiggler periods, is independent of the beam energy γ under the same wiggler parameters, for all the spectral types. Our results have been obtained for radiation fields of constant amplitude. Inclusion of the time evolution for both the carrier and the sidebands will modify the detrapping rates by changing both the diffusion rate as well as the size of the separatrix. This subject is left for future investigation.

ACKNOWLEDGEMENT

This work was supported by SDIO and managed by SDC.

APPENDIX A: TRANSFORMATIONS IN ACTION-ANGLE VARIABLES

The relations between $\tilde{\gamma}$, ψ and the action-angle variables J , θ are given in closed forms in case of an untapered wiggler. Starting from the general expression (11) and using (8) we have,

$$\frac{1}{\pi} \int_{\psi_{mn}}^{\psi_{mx}} d\psi \left(\frac{\gamma_r H_0}{k_w} - V(\psi) \right)^{1/2}, \quad (A1)$$

$$\theta = \frac{\gamma_r k_b(J)}{2k_w} \int_0^{\psi} d\psi' \left(\frac{\gamma_r H_0}{k_w} - \frac{a_w a_r}{k_w} V(\psi') \right)^{-1/2}, \quad (A2)$$

where

$$V(\psi) = \left(\cos\psi + \psi \sin\psi_r \right).$$

Using $H_s = - (a_w a_s / \gamma_r) V(\psi_r)$ we obtain the action at the separatrix,

$$J_s = \left(\frac{a_w a_r}{\gamma_r} \right)^{1/2} \frac{1}{\pi} \int_{\psi_{mn}}^{\psi_{mx}} d\psi \left(V(\psi) - V(\psi_r) \right)^{1/2}.$$

In case of an untapered wiggler $\psi_r = 0$ Eqs. (A1)-(A2) yield,

$$J = \begin{cases} J_s \left(E_2(\lambda) - (1-\lambda^2)E_1(\lambda) \right), & \lambda^2 < 1 \\ 2J_s \lambda E_2\left(\frac{1}{\lambda}\right), & \lambda^2 > 1 \end{cases} \quad (A3)$$

$$J_s = \frac{8}{\pi} \left(\frac{\lambda a_w a_r k_r}{4k_w} \right)^{1/2}, \quad (A4)$$

$$\sin \frac{\psi}{2} = \begin{cases} \lambda \operatorname{sn} \left(\frac{2}{\pi} E_1(\lambda) \theta \right) , & \lambda^2 < 1, \\ \operatorname{sn} \left(\frac{1}{\pi} E_1 \left(\frac{1}{\lambda} \right) \theta \right) , & \lambda^2 > 1, \end{cases} \quad (\text{A5})$$

where E_1 and E_2 are the complete elliptic integrals of the first and second kind, sn is the Jacobi elliptic sine function, and

$$\lambda^2 = \frac{\gamma_r H_0}{2a_w a_r} + \frac{1}{2}, \quad (\text{A6})$$

is the trapping parameter ($\lambda^2 < 1$ for trapped particles). Using $\kappa_b(J) = (\partial J / \partial H_0)^{-1}$ and (A1) we determine the bounce (synchrotron) frequency

$$\kappa_b(J) = \begin{cases} \kappa_b(0) \frac{\pi}{2E_1(\lambda)} , & \lambda^2 < 1 \\ \kappa_b(0) \frac{\pi\lambda}{E_1(1/\lambda)} , & \lambda^2 > 1 \end{cases} \quad (\text{A7})$$

where

$$\kappa_b(0) = \frac{1}{\gamma_r} \left(\frac{\Lambda}{2} a_w a_r k_w k_r \right)^{1/2}, \quad (\text{A8})$$

is the bounce frequency at the bottom of the well. J and λ^2 are mutually related through (A3) - (A6) and they uniquely label the trajectories.

The Fourier coefficients of the expansion (12) can also be expressed in closed form. They are computed by integration in the complex plane around the singularities, utilizing the double periodicity properties of the Jacobi elliptic functions to obtain,

$$Q_n^\pm = -(\pm 1)^n \frac{n\pi^2}{E_1^2(\lambda)} \frac{q^{\frac{n}{2}}}{1 - (-q)^n}, \quad q = \exp \left(\frac{\pi E_1'(\lambda)}{E_1(\lambda)} \right), \quad \lambda^2 < 1, \quad (\text{A9})$$

$$Q_n^{\pm} = - \frac{n\pi^2 \lambda^2}{E_1^2(1/\lambda)} q^n \left(\frac{1}{1-q^{2n}} \pm \frac{1}{1+q^{2n}} \right), \quad q = \exp \left(\frac{\pi E_1'(1/\lambda)}{E_1(1/\lambda)} \right), \quad \lambda^2 > 1$$

for $n \neq 0$ and,

$$Q_0^{\pm} = 2 \frac{E_2(\lambda)}{E_1(\lambda)} - 1 \quad \lambda^2 < 1, \quad Q_0^{\pm} = 1 - 2\lambda^2 \left(1 - \frac{E_2(1/\lambda)}{E_1(1/\lambda)} \right), \quad \lambda^2 < 1,$$

where $E_1'(\lambda^2) \equiv E_1(1 - \lambda^2)$.

APPENDIX B : PHASE AVERAGING OVER CONSTANT J

The phase average $\langle |V(\psi_{mx}) - V(\psi_i)| \rangle$ over constant J is given, for $\psi_r = 0$, by,

$$\begin{aligned} \langle \dots \rangle &= \frac{1}{2\pi} \int_0^{2\pi} d\theta_i \left| \cos \psi_{mx}(J) - \cos \psi_i(J, \theta_i) \right| \\ &= \frac{4}{2\pi} \int_0^{\psi_{mx}} d\psi_i \left(\frac{d\theta_i}{d\psi_i} \right) \left| \cos \psi_{mx}(J) - \cos \psi_i \right|. \end{aligned} \quad (B1)$$

Substituting $d\theta_i/d\psi_i$ from (A2) and using $\cos \psi_{mx} = \gamma_r H(J)/a_w a_r$ one obtains,

$$\begin{aligned} \langle \dots \rangle &= \frac{\gamma_r \kappa_b}{\pi a_w a_r} \int_0^{\psi_{mx}} d\psi_i \left(\frac{\gamma_r H}{k_w} - \frac{a_w a_r}{k_w} \cos \psi_i \right)^{1/2} \\ &= \sqrt{2} \left[\frac{E_2(\lambda^2)}{E_1(\lambda^2)} - (1 - \lambda^2) \right], \end{aligned} \quad (B2)$$

where λ^2 was defined in (A6).

APPENDIX C : COMPUTATION OF THE QUASILINEAR DIFFUSION COEFFICIENT

We consider the evolution of the electron distribution in the presence of a sideband wave package,

$$a_s(z, t) = \frac{1}{2\pi} \int dk_s a_s(k_s) e^{ik_s z - i\omega(k_s)t}, \quad (C1)$$

of width Dk_s . The interaction Hamiltonian in action-angle variables, derived in Sec. IV.(b) is,

$$H(J, \theta; z) = H_0(J) + \frac{a_w}{\gamma_r} \sum_{m=0}^{\infty} Q_n^{\pm}(J) \int dk_s a_s(k_s) \cos [n\theta \pm \delta(k_s)z]. \quad (C2)$$

The evolution of the distribution function $f(J, \theta; z)$, under the Hamiltonian flow,

$$\frac{d\theta}{dz} = \frac{\partial H}{\partial J}, \quad \frac{dJ}{dz} = - \frac{\partial H}{\partial \theta}, \quad (C3)$$

is given by,

$$\frac{\partial f}{\partial z} + \frac{d\theta}{dz} \frac{\partial f}{\partial \theta} + \frac{dJ}{dz} \frac{\partial f}{\partial J} = 0. \quad (C4)$$

We separate the distribution $f(J, \theta; z)$ into a slowly varying part $f_0(J; z) = \langle f \rangle$ and a fluctuating part $\delta f(J, \theta; z) = f - \langle f \rangle$. The averaging operator is defined by,

$$\langle f \rangle = \int_0^L \frac{dz}{L} \int_0^{2\pi} \frac{d\theta}{2\pi} f.$$

It is implied in the above definition that the characteristic length for $f_0(J; z)$ is longer than the synchrotron length $L = 2\pi/\kappa_b$. We then obtain from (C4),

$$\frac{\partial \tilde{f}}{\partial z} + \frac{d\theta}{dz} \frac{\partial \tilde{f}}{\partial \theta} + \frac{dJ}{dz} \frac{\partial \tilde{f}}{\partial J} = - \frac{dJ}{dz} \frac{\partial f_0}{\partial J} - \frac{\partial}{\partial J} \left[\frac{dJ}{dz} \tilde{f} - \left\langle \frac{dJ}{dz} \tilde{f} \right\rangle \right], \quad (C5)$$

$$\frac{\partial}{\partial z} f_0 = - \frac{\partial}{\partial J} \left\langle \frac{dJ}{dz} \tilde{f} \right\rangle. \quad (C6)$$

Using Eqs. (C2) and (C3) inside Eq. (C5) and ignoring the last bracketed term in the right-hand side we obtain,

$$\tilde{f} = - \frac{a_w}{2\gamma_r} \sum_{n=1}^{\infty} \int dk_s \frac{n Q_n^{\pm}(J) a_s(k_s)}{n \kappa_b(J) \pm \delta(k_s)} \frac{\partial f_0}{\partial J} e^{i[n\theta \pm \delta(k_s)]} + cc. \quad (C7)$$

Substituting (C7) in (C6) we have,

$$\begin{aligned} \frac{\partial}{\partial z} f_0 &= \frac{1}{(2\pi)^2} \int_{-\infty}^{\infty} dk_s \int_{-\infty}^{\infty} dq_s \int_0^L \frac{dz}{L} \int_0^{2\pi} \frac{d\theta}{2\pi} \frac{a_w^2}{4\gamma_r^2} \\ &\times \frac{\partial}{\partial J} \left\{ \left[\sum_{m=0}^{\infty} i m Q_m^{\pm}(J) a_s(q_s) e^{i[m\theta \pm \delta(q_s)z]} + cc \right] \right. \\ &\left. \left[\sum_{n=0}^{\infty} \frac{n Q_n^{\pm}(J) a_s(k_s)}{n \kappa_b(J) \pm \delta(k_s)} \frac{\partial f_0}{\partial J} e^{i[n\theta \pm \delta(k_s)]} + cc \right] \right\}, \end{aligned} \quad (C8)$$

where again $\delta(k_s) = (k_w/k_r)[(k_s - k_r) + i\varepsilon]$, $\varepsilon = \text{Im}(k_s)$. Integration of the right-hand side of (C8) over θ yields,

$$\int_0^{2\pi} \frac{d\theta}{2\pi} \left\{ \dots \right\} = - \sum_{n=0}^{\infty} \left[i \frac{|Q_n^{\pm}|^2 a_s^*(q_s) a_s(k_s)}{n \kappa_b(J) \pm \delta(k_s)} e^{\pm[\delta^*(q_s) - \delta(k_s)]z} + cc \right]. \quad (C9)$$

Spatial integration yields

$$\frac{1}{L} \int_0^L dz a^*(q_s) a(k_s) e^{\pm \frac{k_w}{k_r} [(q_s - k_s) + 2 i \epsilon] z} = 2\pi W(q_s, z) \delta(q_s - k_s), \quad (C10)$$

where $W_k(z) = a^2(k_s, z)/L$ is the spectral energy density. Substitution of the results (C9) and (C10) back in (C8) yields,

$$\frac{\partial f}{\partial z} = \frac{\partial}{\partial J} D_q(J) \frac{\partial f}{\partial J},$$

where

$$D_q(J) = \frac{k_r}{4\pi} \frac{a_w^2}{\gamma_r^2} \frac{k_r}{k_w} \sum_{n=1}^{\infty} \int dk_s \frac{n^2 W_{k_s}(z) |Q_n^{\pm}|^2 \epsilon}{\left[\frac{k_r}{k_w} n \kappa_b(J) \pm (k_s - k_r) \right]^2 + \epsilon}. \quad (C11)$$

In the limit of small growth rate $\epsilon/k_s \ll 1$, (C11) is reduced to Eq. (42), Sec. IV,

$$D_q(J) = \frac{k_r}{4} \frac{k_r}{k_w} \frac{a_w^2}{\gamma_r^2} \sum_{n=0}^{\infty} |Q_n^{\pm}|^2 \int_{-\infty}^{\infty} dk_s W_{k_s}(z) \delta(k_s - k_n), \quad (C12)$$

where $k_n = k_r \pm 2\gamma_z^2 k_w$.

APPENDIX D: SUMMATION OF FOURIER COEFFICIENTS

We present a general technique of computing sums of the form,

$$\sum_{n=0}^{\infty} n^2 \left[|Q_n^+(J)|^2 + |Q_n^-(J)|^2 \right]. \quad (D1)$$

The quantities $Q_n^{\pm}(J)$ are the Fourier coefficients from the decomposition of the phase $\exp[i\psi(J,\theta)]$ of the perturbation into harmonics of the angle variable θ for the unperturbed system. The knowledge of the individual $Q_n^{\pm}(J)$ is not required in the computation. The technique should be applicable to a wide class of integrable systems experiencing a periodic perturbation with only minor modifications. In our case $Q_n^{\pm}(J)$ are defined by,

$$\cos [\psi(J,\theta) + \delta_s z] = \sum_{n=0}^{\infty} Q_n^+(J) \cos(n\theta + \delta_s z) + Q_n^-(J) \cos(n\theta - \delta_s z). \quad (D2)$$

Closed forms for $Q_n^{\pm}(J)$, obtained in Ref. 2 for the case of an untapered wiggler, appear in Appendix A.

For untrapped particles we have,

$$Q_{2m}^{\pm} = Q_{2m}, \quad Q_{2m+1}^{\pm} = \pm Q_{2m+1}.$$

Setting $\delta_s = 0$ in (D2) and differentiating in θ , we obtain,

$$\frac{\partial}{\partial \theta} \cos \psi = - \frac{d\psi}{d\theta} \sin \psi = - \sum_{m=1}^{\infty} (2m) 2Q_{2m} \sin 2m\theta, \quad (D3a)$$

$$\frac{\partial}{\partial \theta} \sin \left[\theta - \frac{\pi}{2} \right] = \frac{d\psi}{d\theta} \cos q = \sum_{m=0}^{\infty} (2m+1) 2Q_{2m+1} \cos[(2m+1)\theta]. \quad (D3b)$$

Squaring the right-hand sides of (D3a), (D3b), adding them and integrating over θ we obtain,

$$\sum n^2 \left[|Q_n^+|^2 + |Q_n^-|^2 \right] = 2 \sum n^2 |Q_n|^2 = \frac{1}{2\pi} \int_0^{2\pi} \left(\frac{d\psi}{d\theta} \right)^2 (\cos^2 \psi + \sin^2 \psi) d\theta \quad (D4)$$

Applying the same procedure to untrapped particles we obtain,

$$\frac{\partial}{\partial \theta} \cos \psi = - \frac{d\psi}{d\theta} \sin \psi = - \sum_{n=1}^{\infty} n (Q_n^+ + Q_n^-) \sin n\theta, \quad (D5a)$$

$$\frac{\partial}{\partial \theta} \sin \left[\theta - \frac{\pi}{2} \right] = \frac{d\psi}{d\theta} \cos q = - \sum_{n=0}^{\infty} n (Q_n^+ - Q_n^-) \cos n\theta, \quad (D5b)$$

and, after squaring, adding (D5a) and (D5b) and integrating over θ ,

$$\begin{aligned} \sum_{n=0}^{\infty} n^2 \left(|Q_n^+|^2 + |Q_n^-|^2 \right) &= \sum_{n=0}^{\infty} \frac{n^2}{2} \left(|Q_n^+ + Q_n^-|^2 + |Q_n^+ - Q_n^-|^2 \right) \\ &= \frac{1}{2\pi} \int_0^{2\pi} \left(\frac{d\psi}{d\theta} \right)^2 (\cos^2 \psi + \sin^2 \psi) d\theta. \end{aligned} \quad (D6)$$

Thus in both cases,

$$\sum_{n=0}^{\infty} n^2 \left(|Q_n^+|^2 + |Q_n^-|^2 \right) = \frac{1}{2\pi} \int_0^{2\pi} \left(\frac{d\psi}{d\theta} \right)^2 d\theta. \quad (D7)$$

Using the definition Eq. (11) for $\theta(\psi)$, and Eq. (8) for the unperturbed Hamiltonian ($a_s = 0$) in the right-hand side of (D7) we have,

$$\begin{aligned}
\frac{1}{2\pi} \int_0^{2\pi} \left(\frac{d\psi}{d\theta} \right)^2 d\theta &= \frac{1}{2\pi} 2 \int_{\psi_{mn}}^{\psi_{mx}} \frac{d\psi}{\left(\frac{d\theta}{d\psi} \right)} \\
&= \frac{2 k_w}{\gamma_r \omega_b(J)} \frac{1}{\pi} \int_{\psi_{mn}}^{\psi_{mx}} d\psi \left(\frac{\gamma_r H_0(J)}{k_w} - \frac{a_w a_r}{k_w} [\cos\psi + \psi \sin\psi_r] \right)^{1/2}.
\end{aligned} \tag{D8}$$

The last integral in (D8) is by the definition (11) the action J for the unperturbed Hamiltonian, yielding the final result,

$$\sum_{n=0}^{\infty} n^2 (|q_n^+|^2 + |q_n^-|^2) = \frac{2 k_w}{\gamma_r \omega_b(J)} J. \tag{D9}$$

REFERENCES

1. N. M. Kroll, P. L. Morton and M. N. Rosenbluth, IEEE Journal Quantum Electronics, QE-17, 1436 (1981).
2. S. Riyopoulos and C. M. Tang, in Proceedings of the Eighth International FEL Conference, Glasgow, Scotland, edited by M. Poole (North Holland, Amsterdam, 1987), p. 226.
3. S. S. Yu, W. M. Sharp, W. M. Fawley, E. T. Scharlemann, A. M. Sessler and E. J. Sternbach, in Proceedings of the Eighth International FEL Conference, Glasgow, Scotland, edited by M. Poole (North Holland, Amsterdam, 1987), p. 219.
4. R. C. Davidson and J. S. Wurtele, Phys. Fluids 30, 557 (1987).
5. R. C. Davidson and J. S. Wurtele, Phys. Fluids 30, 2825 (1987).
6. T. Masud, T. C. Marshall, S. P. Schlesinger and F. G. Yee, Phys. Rev. Lett. 56, 1567 (1986).
7. T. Masud, T. C. Marshall, S. P. Schlesinger, F. G. Yee, W. M. Fawley, E. T. Scharlemann, S. S. Yu, A. M. Sessler and E. J. Sternbach, to appear in Transactions on Plasma Science (1988).
8. C. M. Tang and P. Sprangle in Proceedings, Free Electron Generators of Coherent Radiation, Orcas Island, Washington, edited by S. F. Jacobs and M. O. Scully, 1983, (SPIE, Bellingham, WA, 1983), Vol. 453, p. 11.
9. W. B. Colson, in Proceedings of The Seventh International FEL Conference, Tahoe City, edited by E. T. Scharlemann and D. Prosnitz (North Holland, Amsterdam, 1985), p. 168; also W. B. Colson, in Proceedings of the International Conference on Lasers, (STS Press, McLean, VA, 1982) p. 751.

10. J. C. Goldstein, B. E. Newnam, R. W. Warren and R. L. Sheffield, in Proceedings of The Seventh International FEL Conference, Tahoe City, edited by E. T. Scharlemann and D. Prosnitz (North Holland, Amsterdam, 1985), p. 4; also R. W. Warren, J. C. Goldstein and B. E. Newnam, same as above, p. 19.
11. D. C. Quimby, J. M. Slater and J. P. Wilcoxon, IEEE J. Quant. Elec. 21, 979 (1986).
12. See, for example, A. J. Lichtenberg and M. A. Lieberman, Regular and Stochastic Motion (Springer-Verlag, New York, 1983), and references therein.
13. H. Poincare, New Methods of Celestial Mechanics, (Dover, New York, 1957).
14. B. V. Chirikov, Phys. Reports 52, 265 (1979)
15. P. Sprangle and C. M. Tang, Phys. Fluids 28, 2019 (1985).
16. P. Sprangle, A. Ting and C. M. Tang, Phys. Rev. Lett. 59, 202 (1987).
17. P. Sprangle, A. Ting and C. M. Tang, Phys. Rev. A36, 2773 (1987).
18. In case of a tapered wiggler, there is a jump ΔJ in action on crossing a boundary in phase space between two untrapped particle regimes. Since J also parametrizes the distance from a given island center ψ_r , the jump ΔJ reflects the shift in the fixed point $\psi_r \rightarrow \psi_r + 2\pi$ from which we measure this distance.
19. A. K. Ram, K. Hizanidis and A. Bers, Phys. Rev. Lett. 56, 147 (1986).
20. A. Vedenov, E. Velikhov and R. Z. Sagdeev, Nucl. Fusion 1, 82 (1961); also W. E. Drummond and D. Pines, Nucl. Fusion, Suppl. 3, 1049 (1962).

21. C. F. Kennel and F. Engelmann, Phys. Fluids 9, 2377 (1966).
22. C. F. F. Karney, Phys. Fluids 21, 1584 (1978).

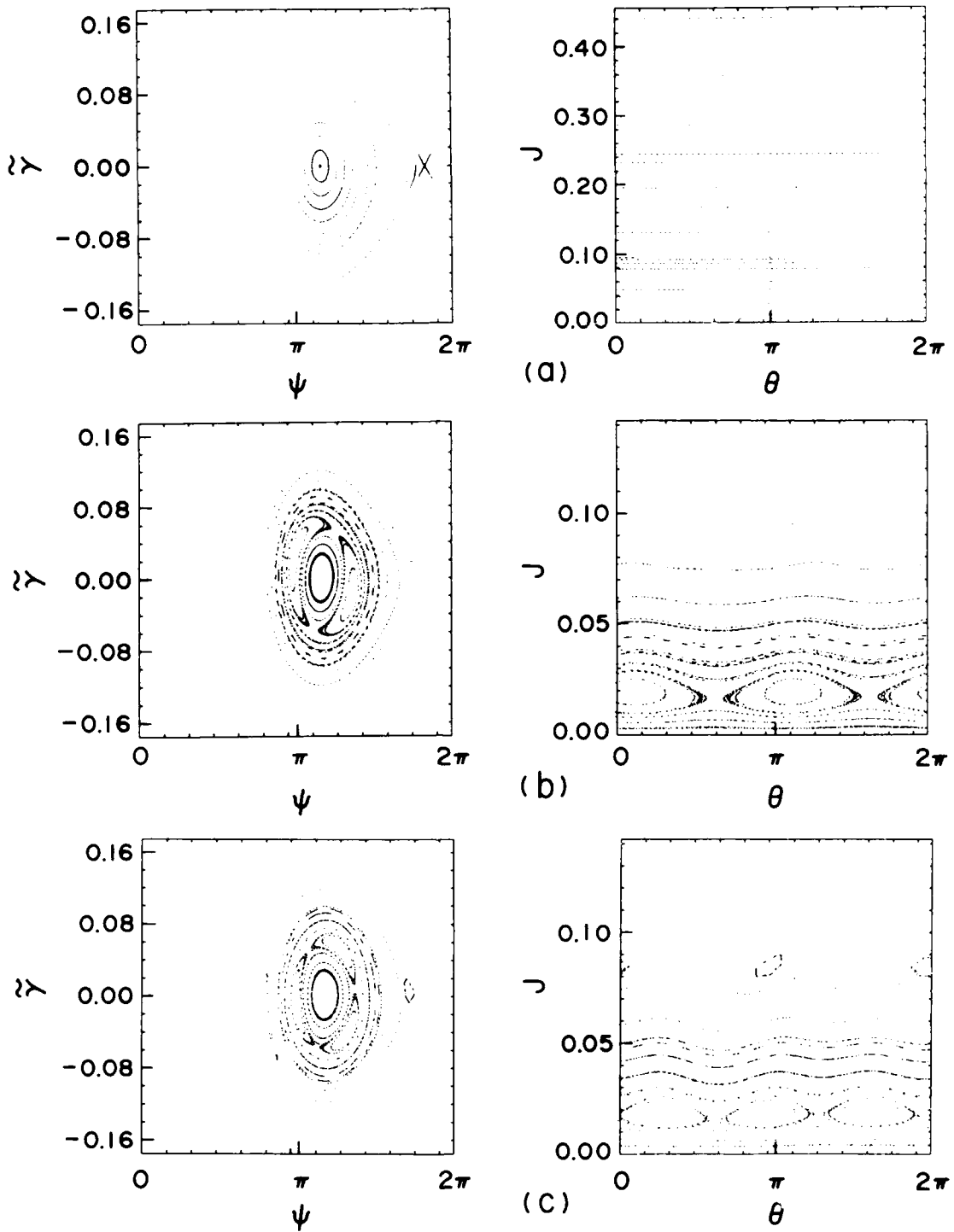


Figure 1. Surfaces of section expressed in γ, ψ coordinates on the left side and action-angle coordinates on the right side. The parameters are $a_w = 2$, $a_r = 5 \times 10^{-5}$, $\psi_r = 7\pi/6$, $\gamma_r = 25$ and (a) $a_s = 0$, (b) $a_s = 5 \times 10^{-7}$, $\omega_s/\omega_r = 1.016$, (c) $a_s = 2 \times 10^{-6}$, $\omega_s/\omega_r = 1.024$.

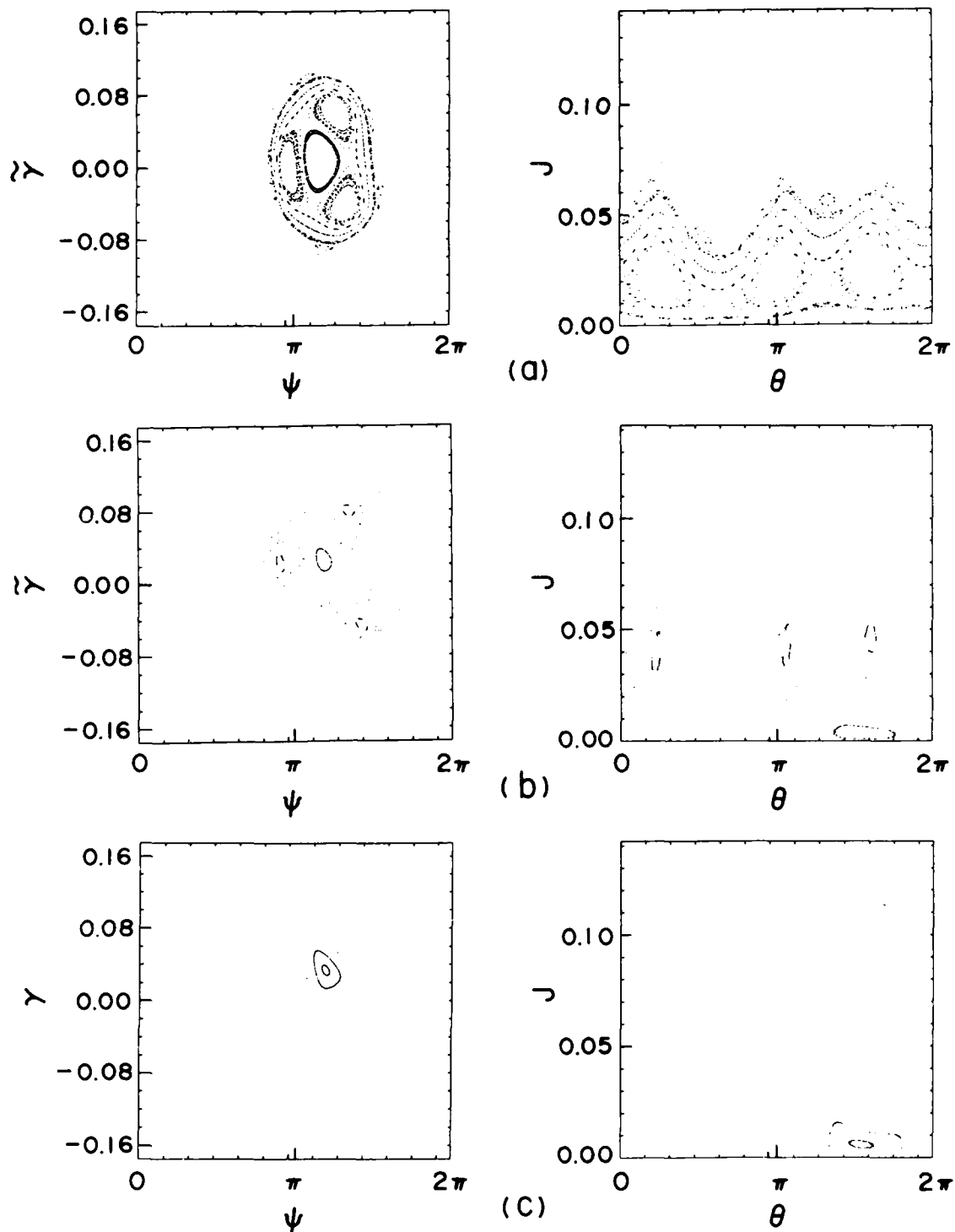


Figure 2. Transition to chaotic behavior. Plotted again are surfaces of section in both $\tilde{\gamma}, \psi$ and J, θ representations. The parameters are $a_w = 2$, $a_r = 5 \times 10^{-5}$, $\psi_r = 7\pi/6$, $\gamma_r = 25$ and $\omega_s/\omega_r = 1.024$. The sideband amplitude increases from (a) $a_s = 1 \times 10^{-5}$ to (b) $a_s = 3 \times 10^{-5}$ to (c) $a_s = 5 \times 10^{-5}$.

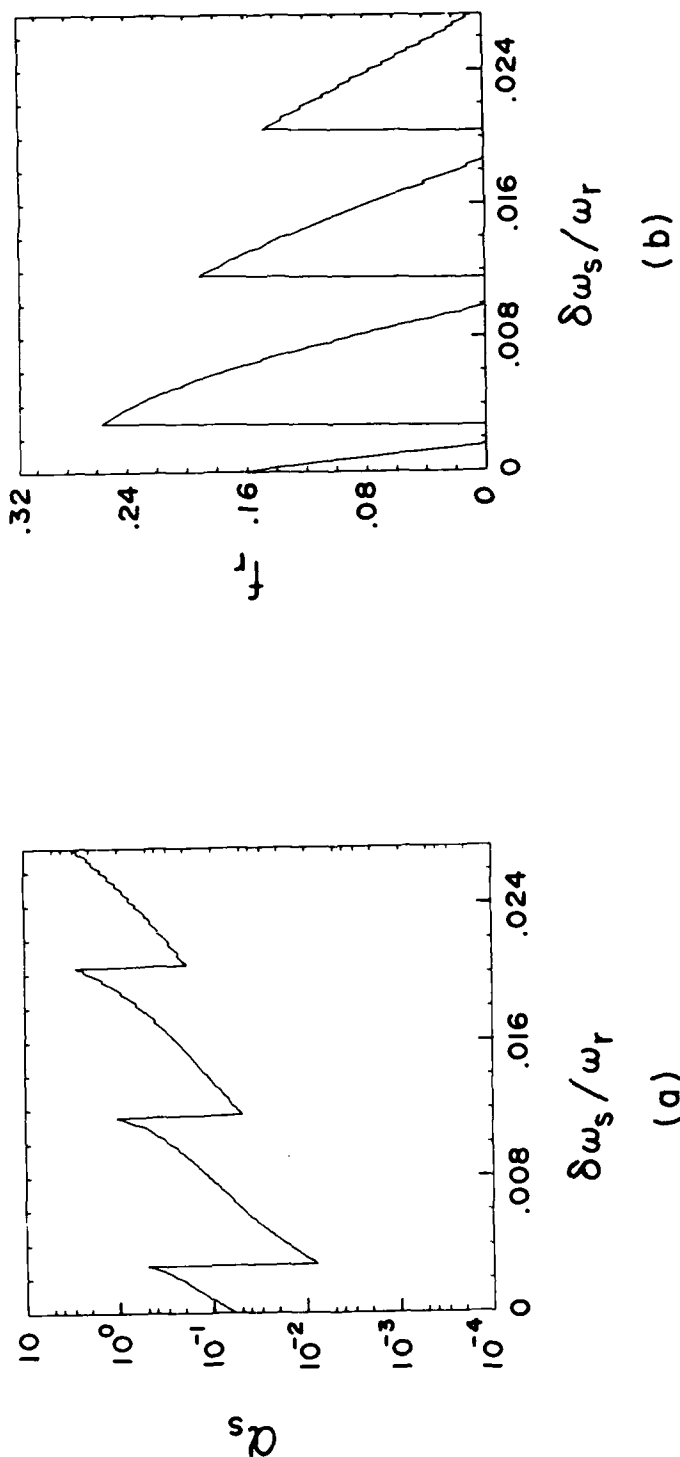


Figure 3. Stochasticity threshold α_s for single frequency sideband.

(a) Plot of α_s against the sideband frequency mismatch $\delta\omega/\omega_r$ (solid line), signifying the overlapping of the two innermost secondary island chains (extended stochastic behavior). The dashed line α_s' signifies the overlapping of the next two islands on the outside (limited stochastic behavior). (b) The fraction f_s of the phase area inside the separatrix that remains integrable when $a_s = \alpha_s$ (solid) and when $a_s = \alpha_s'$ (dashed) line.

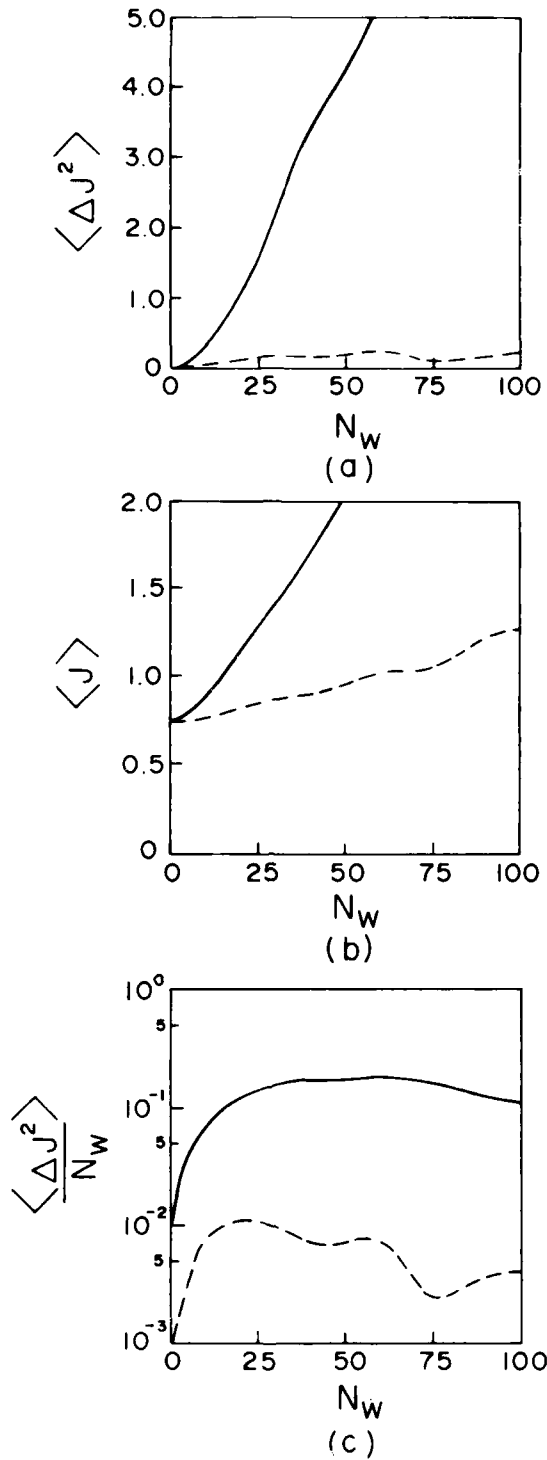


Figure 4. Diffusive behavior of a "monoenergetic" initial distribution $J_0 = 0.7 J_s$ with $a_w = 2$, $a_r = 5 \times 10^{-5}$, $\psi_r = 7\pi/6$, $\gamma_r = 25$ and $\omega_s/\omega_r = 1.016$. Plotted are (a) $\langle \Delta J^2 \rangle$ (b) $\langle J \rangle$ and (c) $\langle \Delta J^2 \rangle / z$ as functions of $N_w = z / \lambda_w$. The solid curves correspond to $a_s = 1.5 \times 10^{-5}$ and the dashed ones to $a_s = 5 \times 10^{-5}$.

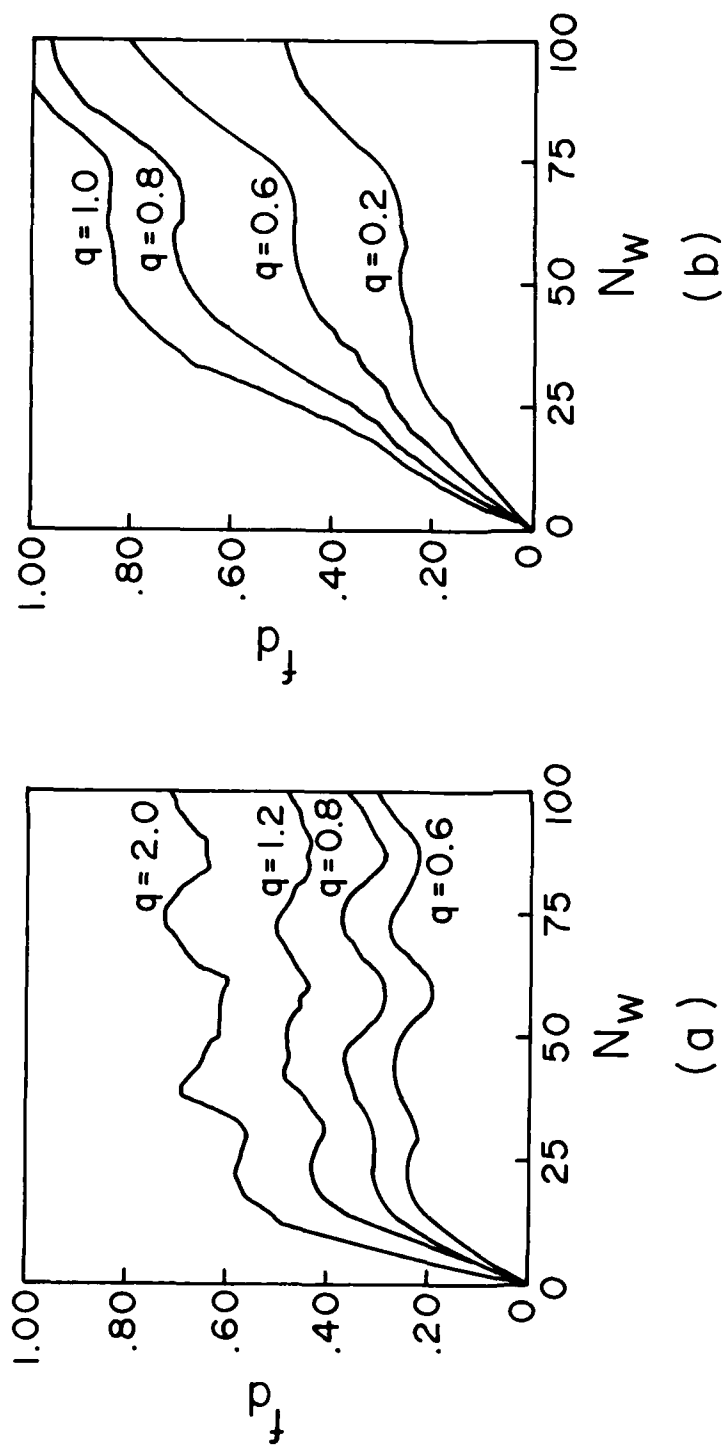


Figure 5. The fraction f_d of detrapped particles against the distance in wiggler periods $N_w = z / \lambda_w$. Different curves correspond to various sidebands to carrier amplitude ratios $q = a_s/a_r$. Parameters are $a_w = 2$, $a_r = 5 \times 10^{-5}$, $\psi_r = 7\pi/6$, $\gamma_r = 25$ and (a) $\omega_s/\omega_r = 1.016$, (b) $\omega_s/\omega_r = 1.024$.

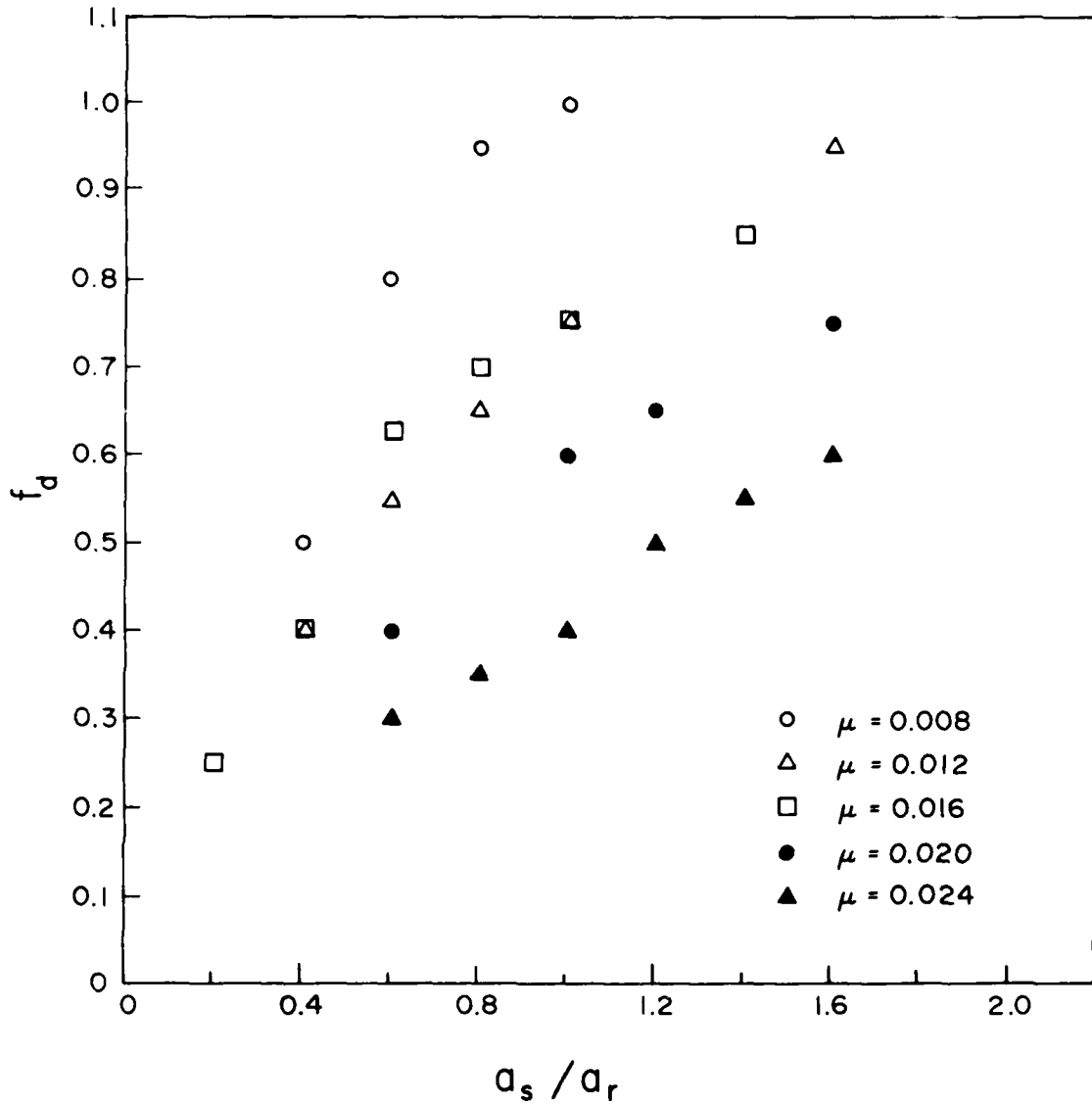


Figure 6. The fraction f_d of detrapped particles after 100 wiggler periods for an initially uniformly filled bucket. Results for various sideband frequency ratios $\mu = \omega_s/\omega_r$ are plotted against the relative sideband amplitude $q = a_s/a_r$ for $a_w = 2$, $a_r = 5 \times 10^{-5}$ and $\psi_r = 7\pi/6$, $\gamma_r = 25$.

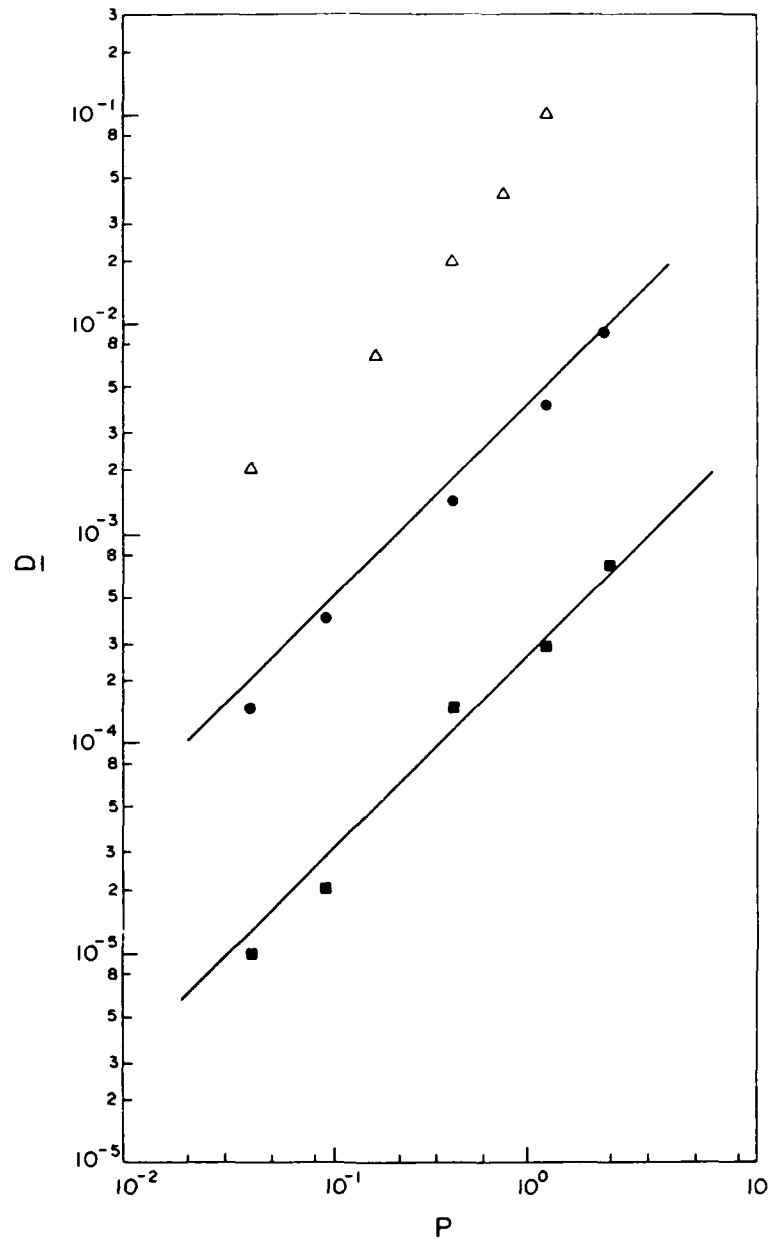


Figure 7. The normalized diffusion coefficient \underline{D} as a function of the sideband power ratio $P = W_S/W_R$ for $a_w = 2$, $a_r = 5 \times 10^{-5}$ and $\psi_r = 7\pi/6$, $\gamma_r = 25$. Squares correspond to a continuous type of spectrum, peaked at $\omega_s/\omega_r = 1.016$ with $A = 100$ and $\nu = 0.1$. Dots correspond to a wide discrete peaked at $\omega_s/\omega_r = 1.024$ with $A = 20$ and $\nu = 0.5$. Triangles correspond to a single frequency spectrum with $\omega_s/\omega_r = 1.016$. The upper and lower solid lines correspond to the theoretical results from Eqs. (36) and (42) respectively.

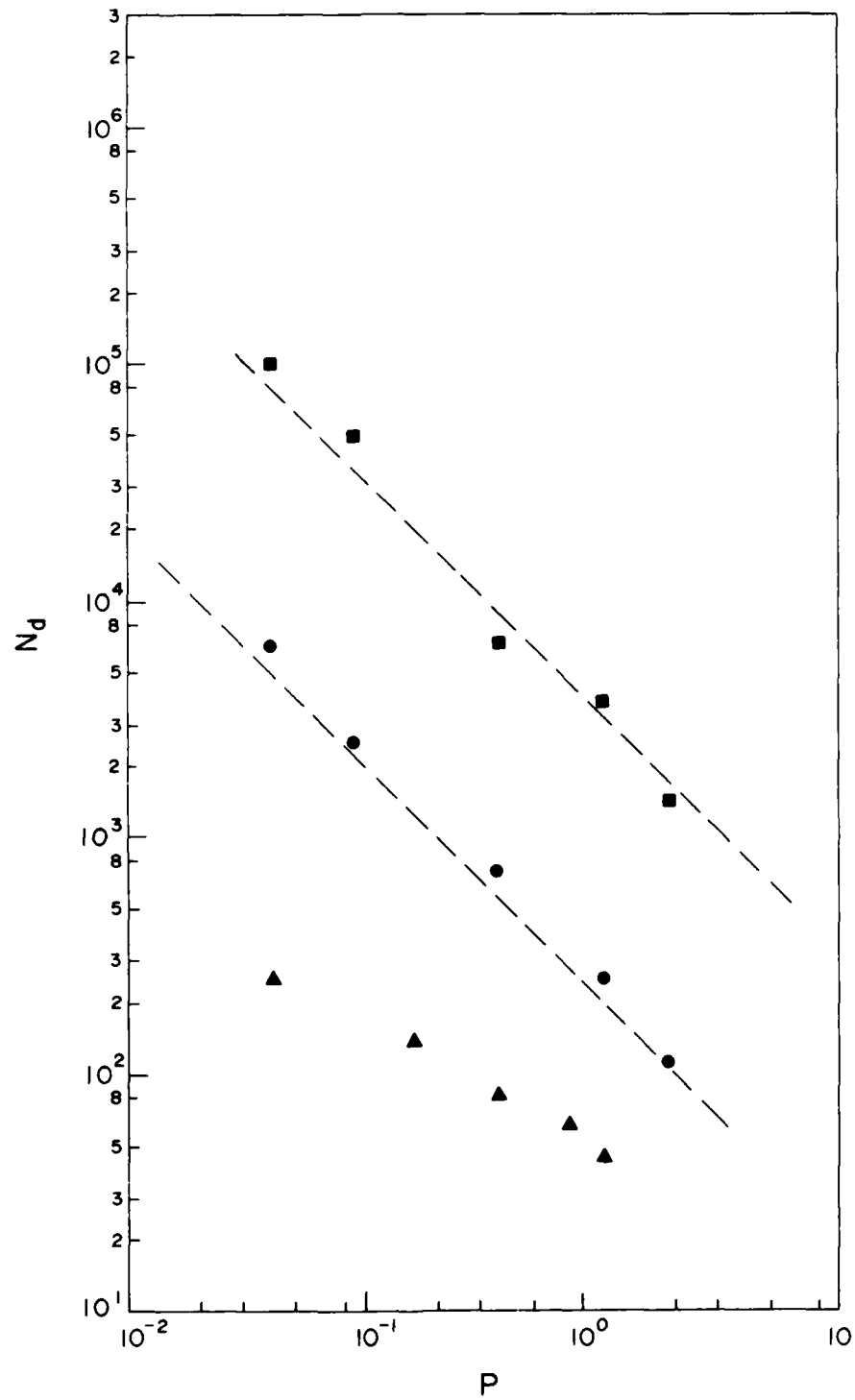


Figure 8. The e-folding diffusion length N_d in wiggler periods for the number of trapped particles. Parameters and semantics are the same as in Fig. 7.

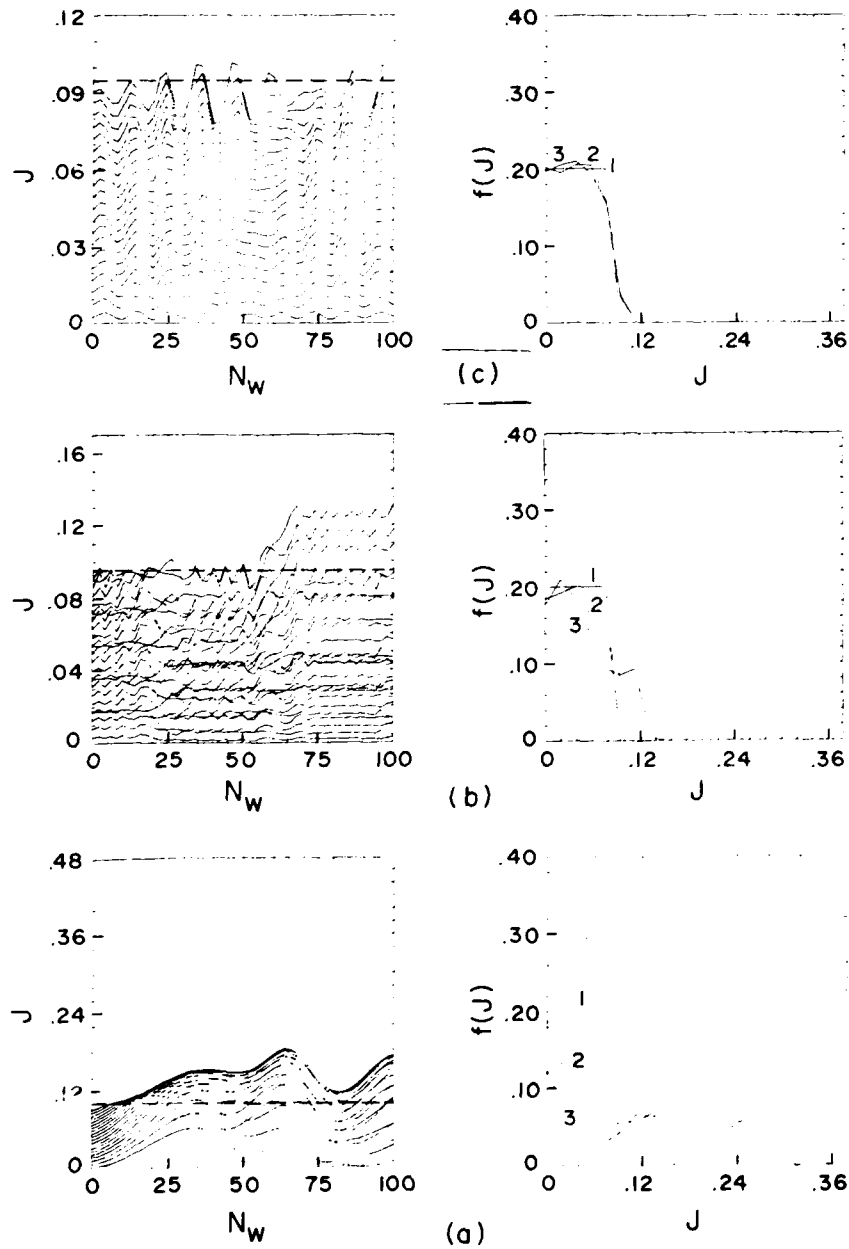


Figure 9. Particle response under different sideband spectra. On the left-hand side we plot the action J against the number of wiggler periods N_w for selected particles. On the right-hand side we plot the corresponding distribution function $f(J)$ at $N_w = 0, 50$, and 100 . In all cases the total sideband power ratio $P = W_s/W_r = 0.36$ and $a_w = 2$, $a_r = 5 \times 10^{-5}$, $\gamma_r = 25$. (a) corresponds to a wide continuous sideband spectrum (b) corresponds to a wide discrete spectrum and (c) to a single frequency $\omega_s/\omega_r = 1.016$.

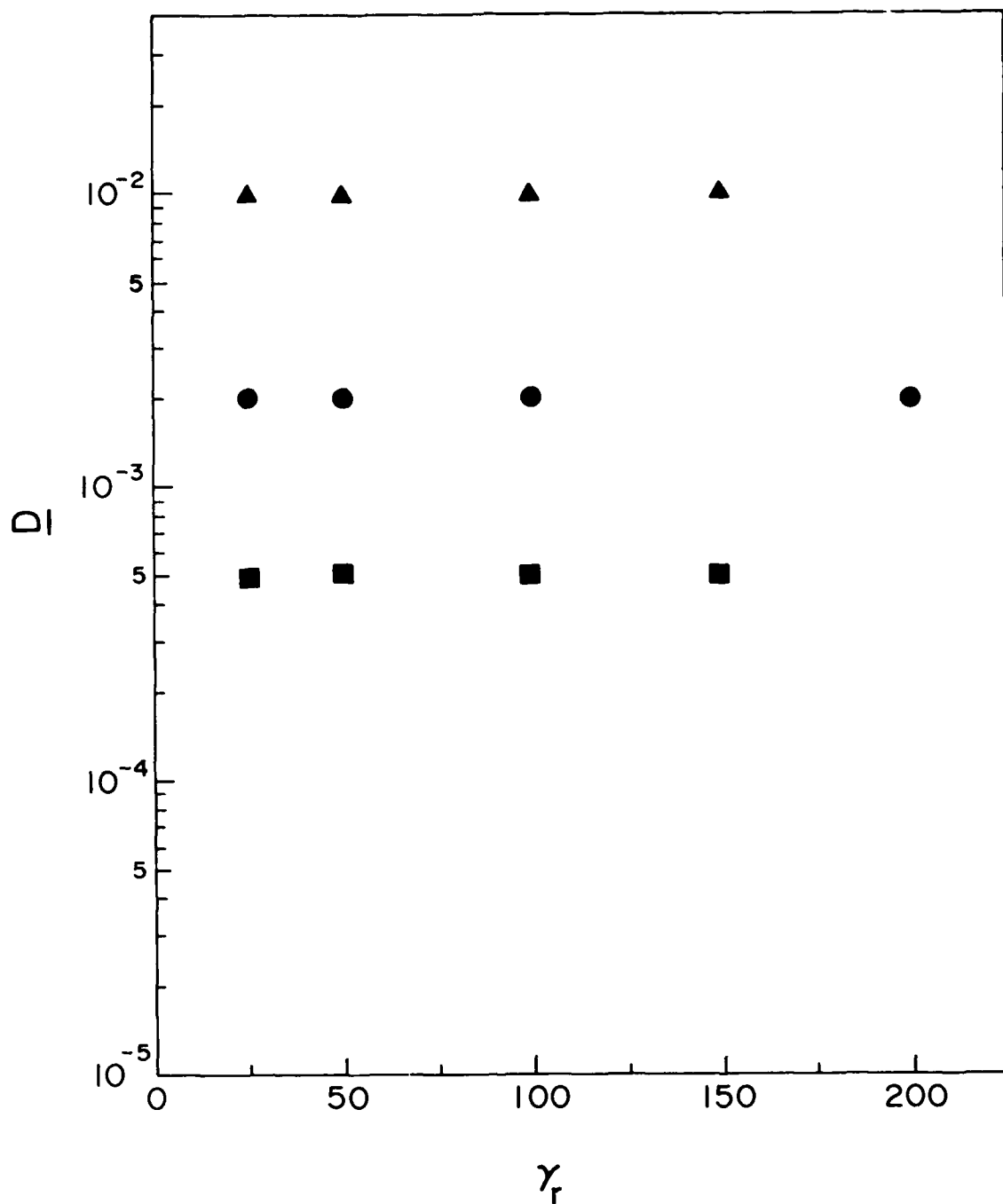


Figure 10. Plots of the normalized diffusion coefficient \underline{D} against the electron energy γ_r . Parameters are $a_w = 2$, $a_r = 2 \times 10^{-4}$, $a_s = 7.5 \times 10^{-5}$ and $\omega_s = 1.024$. Squares correspond to a continuous, dots to a wide discrete and triangles to a single frequency spectrum.

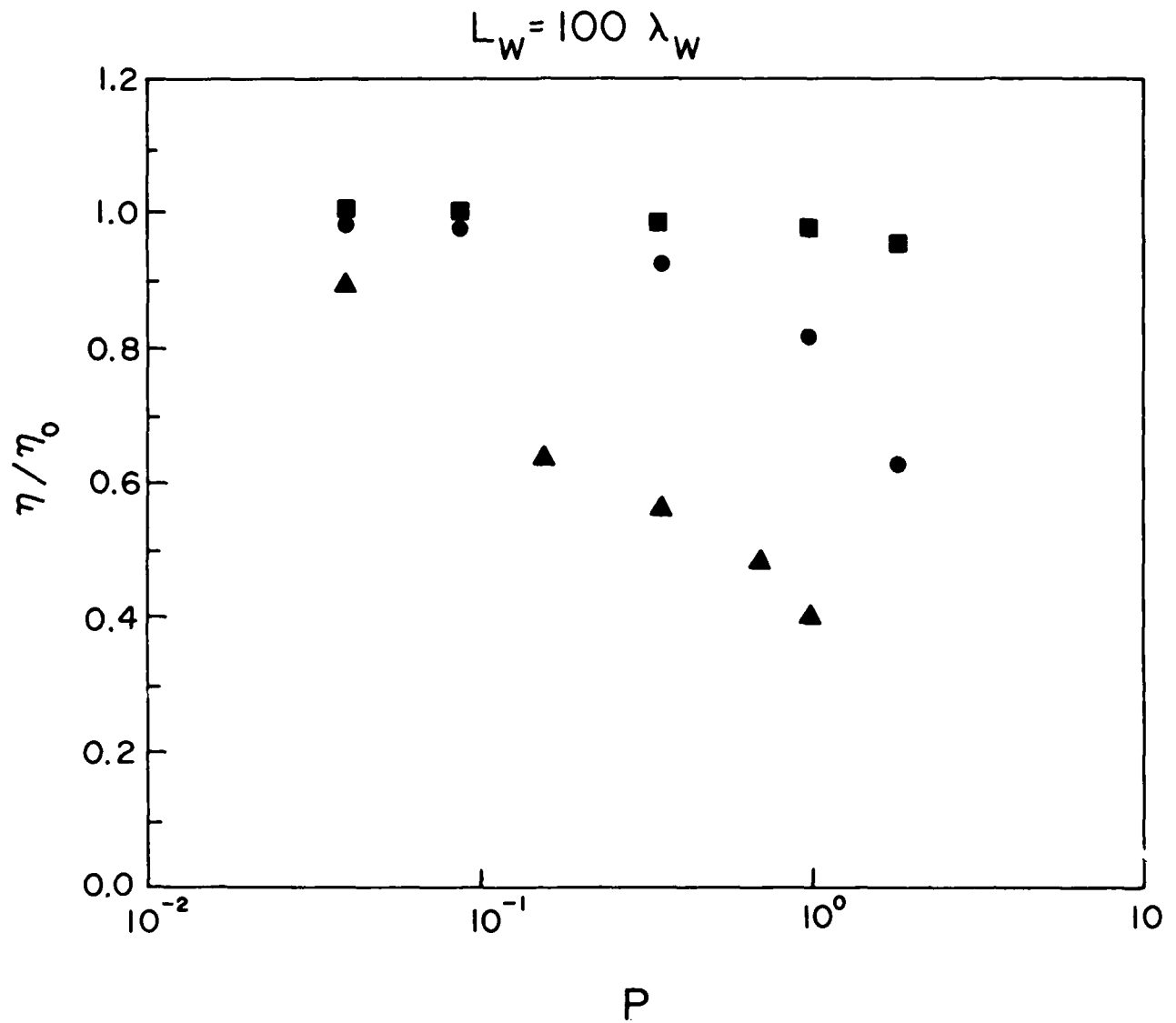


Figure 11. Deterioration of the extraction efficiency for various spectral types. Plotted is the ratio η/η_0 for a wiggler length of 100 periods as a function of the sideband power ratio P . The numerical results in Fig. 8 were used in Eq. (49) to create this plot. The symbolism and the parameters are the same as in Fig. 8.

DISTRIBUTION LIST*

Naval Research Laboratory
4555 Overlook Avenue, S.W.
Washington, DC 20375-5000

Attn: Code 1000 - Commanding Officer, CAPT W. G. Clautice
1001 - Dr. T. Coffey
1005 - Head, Office of Management & Admin.
1200 - CAPT M. A. Howard
1220 - Mr. M. Ferguson
2000 - Director of Technical Services
2604 - NRL Historian
4000 - Dr. W. R. Ellis
4600 - Dr. D. Nagel
4603 - Dr. W. W. Zachary
4700 - Dr. S. Ossakow (26 copies)
4700.1-Dr A. W. Ali
4710 - Dr. C. A. Kapetanakos
4730 - Dr. R. Elton
4740 - Dr. W. M. Manheimer
4740 - Dr. W. Black
4740 - Dr. J. Condon
4740 - Dr. A. W. Fliflet
4740 - Dr. S. Gold
4740 - Dr. D. L. Hardesty
4740 - Dr. A. K. Kinhead
4740 - Dr. M. Rhinewine
4770 - Dr. G. Cooperstein
4790 - Dr. P. Sprangle
4790 - Dr. C. M. Tang (20 copies)
4790 - Dr. M. Lampe
4790 - Dr. Y. Y. Lau
4790A- W. Brizzi
5700 - Dr. L. A. Cosby
6840 - Dr. S. Y. Ahn
6840 - Dr. A. Ganguly
6840 - Dr. R. K. Parker
6843 - Dr. R. H. Jackson
6843 - Dr. N. R. Vanderplaats
6843 - Dr. C. M. Armstrong
6875 - Dr. R. Wagner
2628 - Documents (22 copies)

NRL Records 1 copy
2634 C. Sims 1 copy

* Every name listed on distribution gets one copy except for those where extra copies are noted.

Dr. R. E. Aamodt
Lodestar Research Corp.
2400 Central Ave., P-5
Boulder, CO 80301

Dr. J. Adamski
Boeing Aerospace Company
P.O. Box 3999
Seattle, WA 98124

Dr. H. Agravante
TRW, Inc.
One Space Park
Redondo Beach, CA 90278 / R1-2020

Prof. I. Alexeff
University of Tennessee
Dept. of Electrical Engr.
Knoxville, TN 37916

Dr. L. Altgilbers
3805 Jamestown
Huntsville, AL 35810

Dr. A. Amir
Quantum Inst. and Dept. of Physics
University of California
Santa Barbara, CA 93106

Dr. Bruce Anderson
Air Force Weapons Laboratory
Kirtland AFB
Albuquerque, NM 87117

Dr. Antonio Anselmo
VARIAN
MS K-416
611 Hanson Way
Palo Alto, CA 94303

Dr. T. M. Antonsen
University of Maryland
College Park, MD 20742

Dr. Tony Armstrong
Science Applications Intl. Corp.
P.O. Box 2351
La Jolla, CA 92038

Dr. Joseph Ashkenazy
M.I.T.
Research Lab. of Electronics
Room 36-219
Cambridge, MA 02139

Assistant Secretary of the
Air Force (RD&L)
Room 4E856, The Pentagon
Washington, D.C. 20330

Dr. W. P. Ballard
Sandia National Laboratories
ORG. 1231, P.O. Box 5800
Albuquerque, NM 87185

Mr. Jon Barber
Dept. of Physics
Bethel College
St. Paul, MN 55112

Dr. W. A. Barletta
Lawrence Livermore National Lab.
P. O. Box 808
Livermore, CA 94550

Dr. John J. Barnard
Lawrence Livermore Nat. Lab.
P. O. Box 808, L-626
Livermore, CA 94550

Dr. L. R. Barnett
3053 Merrill Eng. Bldg.
University of Utah
Salt Lake City, UT 84112

CDR George Bates, PMS 405-300
Naval Sea Systems Command
Department of the Navy
Washington, DC 20362

Dr. W. Becker
Univ. of New Mexico
Institute for Mod. Opt.
Albuquerque, NM 87131

Dr. Robert Behringer
9342 Balcon Ave.
Northridge, CA 91325

Dr. G. Bekefi (5 copies)
Mass. Institute of Tech.
Room 36-213
Cambridge, MA 02139

Dr. S. Bender
Los Alamos National Laboratory
P. O. Box 1663
Los Alamos, NM 87545

Dr. J. Benford
Physics International
2700 Merced Street
San Leandro, CA 94577

Dr. Herbert S. Bennett
National Bureau of Standards
Bldg. 225, Rm. A352
Washington, DC 20234

Dr. Steven V. Benson
Physics Department
Stanford, CA 94305

Dr. T. Berlincourt
Office of Naval Research
Attn: Code 420
Arlington, VA 22217

Dr. I. B. Bernstein (10 copies)
Mason Laboratory
Yale University
400 Temple Street
New Haven, CT 06520

Dr. Vladislav Bevc
Synergy Research Institute
P.O. Box 561
San Ramon, CA 94583

Dr. Amitava Bhattacharjee
Columbia University
S. W. Mudd 210
Dept. of Applied Phys.
New York, NY 10027

Dr. Anup Bhowmik
Rockwell International/Rocketdyne Div.
6633 Canoga Avenue, FA-40
Canoga Park, CA 91304

Dr. K. Jim Bickford
RDA
2301F Yale Blvd., S.E.
Albuquerque, NM 87106

Dr. D. L. Bix
Lawrence Livermore National Laboratory
P. O. Box 808
Livermore, CA 94550

Dr. J. Bisognano
Lawrence Berkeley Laboratory
University of California, Berkeley
Berkeley, CA 94720

Dr. Steve Bitterly
Rockwell International/Rocketdyne Div.
6633 Canoga Avenue, FA-40
Canoga Park, CA 91304

Dr. H. Boehmer
TRW DSSG
One Space Park
Redondo Beach, CA 90278

Dr. John Booske
Energy Research Bldg.
University of Maryland
College Park, MD 20742

Dr. P. Bosco
KMS Fusion Inc.
Ann Arbor, MI 48106

Dr. I. Boscolo
Quantum Institute
University of California
Santa Barbara, CA 93106

Dr. B. Boswell
Lab for Laser Energetics
University of Rochester
250 E. River Road
Rochester, NY 14623

Dr. G. Bourianoff
1901 Rutland Drive
Austin, TX 78758

Dr. J. K. Boyd
Lawrence Livermore National Laboratory
P. O. Box 808
Livermore, CA 94550

Dr. E. Bozoki
NSLS
Brookhaven National Lab.
Upton, NY 11973

Dr. H. Brandt
Department of the Army
Harry Diamond Laboratory
2800 Powder Mill Rd.
Adelphi, MD 20783

Dr. R. Briggs
Lawrence Livermore National Lab.
MS-626
P.O. Box 808
Livermore, CA 94550

Dr. H. L. Buchanan
Defense Advanced Research Projects Agency
1400 Wilson Blvd.
Arlington, VA 22209

Dr. D. L. Bullock
Optical Sciences Department
TRW Space and Technology Group
Redondo Beach, CA 90278

Dr. Fred Burskirk
Physics Department
Naval Postgraduate School
Monterey, CA 93940

Dr. Ken Busby
Mission Research Corporation
1720 Randolph Road, S.E.
Albuquerque, NM 87106

Dr. K. J. Button
Francis Bitter Natl. Magnet Lab.
Box 72, M. I. T. Branch
Cambridge, MA 02139-0901

Dr. J. A. Byers
Lawrence Livermore National Lab.
Attn: (L-630)
P. O. Box 808
Livermore, CA 94550

Dr. Gregory Canavan
Office of Inertial Fusion
U.S. Dept. of Energy
M.S. C404
Washington, DC 20545

Dr. Malcolm Caplan
4219 Garland Drive
Fremont, CA 94536

Dr. Maria Caponi
TRW, Building R-1, Room 1184
One Space Park
Redondo Beach, CA 90278

Dr. B. Carlsten
Los Alamos National Laboratory
MS-H827 AT-7
P. O. Box 1663
Los Alamos, NM 87545

Dr. A. Carmichael
U. S. Army - FTC
P. O. Box 1500
Huntsville, AL 35807-3801

Dr. David Cartwright
Los Alamos National Laboratory
E527
Los Alamos, NM 87545

Dr. J. Cary
University of Colorado
Box 391
Boulder, CO 80309

Prof. William Case
Dept. of Physics
Grinnell College
Grinnell, IA 50112

Mr. Charles Cason
U. S. Army Strategic Def. Command
ATTN: Code CSSD-H-D
P. O. Box 1500
Huntsville, AL 35807-3801

Dr. S. Caspi
Lawrence Berkeley Lab.
Bldg. 46
Berkeley, CA 94720

Dr. R. Center
Spectra Tech., Inc.
2755 Northup Way
Bellevue, WA 98004

Prof. Frank Chan
School of Eng. & Applied Sciences
Univ. of Calif. at Los Angeles
7731 K Boelter Hall
Los Angeles, CA 90024

Dr. K. C. Chan
Los Alamos National Laboratory
P. O. Box 1663
Los Alamos, NM 87545

Dr. V. S. Chan
GA Technologies
P.O. Box 85608
San Diego, CA 92138

Dr. Will E. Chandler
Pacific Missile Test Center
Code 0141-5
Point Muga, CA 93042

Dr. J. Chase
Lawrence Livermore National Laboratory
P. O. Box 808
Livermore, CA 94550

Dr. S. Chattopadhyay
Lawrence Berkeley Laboratory
University of California, Berkeley
Berkeley, CA 94720

Dr. S. Chen
MIT Plasma Fusion Center
NW16-176
Cambridge, MA 01890

Dr. Yu-Juan Chen
L-626
Lawrence Livermore National Laboratory
P. O. Box 808
Livermore, CA 94550

Dr. D. P. Chernin
Science Applications Intl. Corp.
1720 Goodridge Drive
McLean, VA 22102

Dr. Art Chester
Hughes E51
Mail Stop A269
P.O. Box 902
El Segundo, CA 90245

Dr. S. C. Chiu
GA Technologies Inc.
P.O. Box 85608
San Diego, CA 92138

Dr. Y. C. Cho
NASA-Lewis Research Center
Mail Stop-54-5
Cleveland, Ohio 44135

Dr. J. Christiansen
Hughes Aircraft Co.
Electron Dynamics Division
3100 West Lomita Blvd.
Torrance, CA 90509

Dr. T. L. Churchill
Spectra Technology, Inc.
2755 Northup Way
Bellevue, WA 98004

Major Bart Clare
USASDC
P. O. BOX 15280
Arlington, VA 22215-0500

Dr. Melville Clark
8 Richard Road
Wayland, MA 01778

Dr. Robert Clark
P.O. Box 1925
Washington, D.C. 20013

Dr. Alan J. Cole
TRW
One Space Park
Redondo Beach, CA 90278

Dr. William Colson
Berkeley Research Assoc.
P. O. Box 241
Berkeley, CA 94701

Dr. William Condell
Office of Naval Research
Attn: Code 421
800 N. Quincy St.
Arlington, VA 22217

Dr. Richard Cooper
Los Alamos National Scientific
Laboratory
P.O. Box 1663
Los Alamos, NM 87545

Dr. Robert S. Cooper
Director, DARPA
1400 Wilson Boulevard
Arlington, VA 22209

Dr. M. Cornacchia
Lawrence Berkeley Laboratory
University of California, Berkeley
Berkeley, CA 94720

Dr. R. A. Cover
Rockwell International/Rocketdyne Div.
6633 Canoga Avenue, FA-38
Canoga Park, CA 91304

Dr. D. Crandall
ER-55, GTN
Department of Energy
Washington, DC 20545

Dr. Bruce Danly
MIT
NW16-174
Cambridge, MA 02139

Dr. R. Davidson (5 copies)
Plasma Fusion Center
Mass. Institute of Tech.
Cambridge, MA 02139

Dr. John Dawson (4 copies)
Physics Department
University of California
Los Angeles, CA 90024

Dr. David A. G. Deacon
Deacon Research
Suite 203
900 Welch Road
Palo Alto, CA 94306

Dr. Philip Debenham
Center for Radiation Research
National Bureau of Standards
Gaithersburg, MD 20899

Dr. T. L. Deloney
Dept. of Electrical Engineering
Stanford University
Stanford, CA 94305

Deputy Under Secretary of
Defense for R&AT
Room 3E114, The Pentagon
Washington, D.C. 20301

Prof. P. Diamant
Dept. of Electrical Engineering
Columbia University
New York, NY 10027

Dr. N. Dionne
Raytheon Company
Microwave Power Tube Division
Foundry Avenue
Waltham, MA 02154

Director
National Security Agency
Fort Meade, MD 20755
ATTN: Dr. Richard Foss, A42
Dr. Thomas Handel, A243
Dr. Robert Madden, R/SA

Director of Research (2 copies)
U. S. Naval Academy
Annapolis, MD 21402

Dr. T. Doering
Boeing Aerospace Company
P.O. Box 3999
Seattle, WA 98124

Dr. Gunter Dohler
Northrop Corporation
Defense Systems Division
600 Hicks Road
Rolling Meadows, IL 60008

Dr. Franklin Dolezal
Hughes Research Laboratory
3011 Malibu Canyon Rd.
Malibu, CA 90265

Dr. A. Drobot
Science Applications Intl. Corp.
1710 Goodridge Road
McLean, VA 22102

Dr. Dwight Duston
Strategic Defense Initiative Org.
OSD/SDIO/IST
Washington, DC 20301-7100

Dr. Joseph Eberly
Physics Department
Univ. of Rochester
Rochester, NY 14627

Dr. Jim Eckstein
VARIAN
MS K-214
611 Hanson Way
Palo Alto, CA 94303

Dr. J. A. Edighoffer
TRW, Bldg. R-1
One Space Park
Redondo Beach, CA 90278

Dr. O. C. Eldridge
University of Wisconsin
1500 Johnson Drive
Madison, WI 53706

Dr. Luis R. Elias (2 copies)
Creol-FEL Research Pavillion
Suite 400
12424 Research Parkway
Orlando, FL 32826

Dr. C. J. Elliott
Los Alamos National Laboratory
P. O. Box 1663
Los Alamos, NM 87545

Dr. James Elliott
X1-Division, M.S. 531
Los Alamos Natl. Scientific Lab.
P. O. Box 1663
Los Alamos, NM 87545

Dr. A. England
Oak Ridge National Laboratory
P.O. Box Y
Mail Stop 3
Building 9201-2
Oak Ridge, TN 37830

Dr. William M. Fairbank
Phys. Dept. & High Energy
Phys. Laboratory
Stanford University
Stanford, CA 94305

Dr. Anne-Marie Fauchet
Brookhaven National Laboratories
Associated Universities, Inc.
Upton, L.I., NY 11973

Dr. J. Feinstein
Dept. of Electrical Engineering
Stanford University
Stanford, CA 94305

Dr. Frank S. Felber
11011 Torreyana Road
San Diego, CA 92121

Dr. D. Feldman
Los Alamos National Laboratory
P. O. Box 1663
Los Alamos, NM 87545

Dr. Renee B. Feldman
Los Alamos National Laboratory
P. O. Box 1663
Los Alamos, NM 87545

Dr. L. A. Ferrari
Queens College
Department of Physics
Flushing, NY 11367

Dr. C. Finfgeld
ER-542, GTN
Department of Energy
Washington, DC 20545

Dr. A. S. Fisher
Dept. of Electrical Engineering
Stanford University
Stanford, CA 94305

Dr. R. G. Fleig
Hughes Research Laboratory
3011 Malibu Canyon Road
Malibu, CA 90265

Dr. H. Fleischmann
Cornell University
Ithaca, NY 14850

Dr. E. Fontana
Dept. of Electrical Engineering
Stanford University
Stanford, CA 94305

Dr. Norwal Fortson
University of Washington
Department of Physics
Seattle, WA 98195

Dr. Roger A. Freedman
Quantum Institute
University of California
Santa Barbara, CA 93106

Dr. Lazar Friedland
Dept. of Eng. & Appl. Science
Yale University
New Haven, CT 06520

Dr. Walter Friez
Air Force Avionics Laboratory
AFWAL/AADM-1
Wright/Paterson AFB, OH 45433

Dr. Shing F. Fung
Code 696
GSFC
NASA
Greenbelt, MD 20771

Dr. R. Gajewski
Div. of Advanced Energy Projects
U. S. Dept of Energy
Washington, DC 20545

Dr. H. E. Gallagher
Hughes Research Laboratory
3011 Malibu Canyon Road
Malibu, CA 90265

Dr. James J. Gallagher
Georgia Tech. EES-EOD
Baker Building
Atlanta, GA 30332

Dr. W. J. Gallagher
Boeing Aerospace Co.
P. O. Box 3999
Seattle, WA 98124

Dr. J. Gallardo
Quantum Institute
University of California
Santa Barbara, CA 93106

Dr. E. P. Garate
Dept. of Physics and Astronomy
Dartmouth College
Hanover, NH 03755

Dr. A. Garren
Lawrence Berkeley Laboratory
University of California, Berkeley
Berkeley, CA 94720

Dr. Richard L. Garwin
IBM, T. J. Watson Research Ctr.
P.O. Box 218
Yorktown Heights, NY 10598

Dr. J. Gea-Banacloche
Dept. of Physics & Astronomy
Univ. of New Mexico
800 Yale Blvd. NE
Albuquerque, NM 87131

DR. R. I. Gellert
Spectra Technology
2755 Northup Way
Bellevue, WA 98004

Dr. T. V. George
ER-531, GTN
Department of Energy
Washington, DC 20545

Dr. Edward T. Gerry, President
W. J. Schafer Associates, Inc.
1901 N. Fort Myer Drive
Arlington, VA 22209

Dr. Roy Glauber
Physics Department
Harvard University
Cambridge, MA 02138

Dr. B. B. Godfrey
Mission Research Corporation
1720 Randolph Road, S. E.
Albuquerque, NM 87106

Dr. John C. Goldstein, X-1
Los Alamos Natl. Scientific Lab.
P.O. Box 1663
Los Alamos, NM 87545

Dr. Yee Fu Goul
Plasma Physics Lab., Rm 102
S.W. Mudd
Columbia University
New York, NY 10027

Dr. C. Grabbe
Department of Physics
University of Iowa
Iowa City, Iowa 52242

Dr. V. L. Granatstein
Dept. of Electrical Engineering
University of Maryland
College Park, MD 20742

Dr. D. D. Gregoire
Quantum Institute and Dept. of Physics
University of California
Santa Barbara, CA 93106

Dr. Y. Greenzweig
Quantum Inst. and Dept. of Physics
University of California
Santa Barbara, CA 93106

Dr. Morgan K. Grover
R&D Associates
P. O. Box 9695
4640 Admiralty Highway
Marina Del Rey, CA 90291

Dr. A. H. Guenter
Air Force Weapons Laboratory
Kirtland AFB, NM 87117

Lt Col Richard Gullickson
Strategic Def. Initiative Org.
OSD/SDIO/DEO
Washington, DC 20301-7100

Dr. K. Das Gupta
Physics Department
Texas Tech University
Lubbock, TX 79409

Dr. Benjamin Haberman
Associate Director, OSTP
Room 476, Old Exe. Office Bldg.
Washington, D.C. 20506

Dr. R. F. Hagland, Jr.
Director, Vanderbilt University
Nashville, TN 37235

Dr. K. Halbach
Lawrence Berkeley Laboratory
University of California, Berkeley
Berkeley, CA 94720

Dr. P. Hammerling
La Jolla Institute
P.O. Box 1434
La Jolla, CA 92038

Dr. John Hammond
Director, Directed Energy Office
SDIO
The Pentagon, T-DE Rm. 1E180
Washington, DC 20301-7100

Dr. R. Harvey
Hughes Research Laboratory
3011 Malibu Canyon Road
Malibu, CA 90265

Prof. Herman A Haus
Mass. Institute of Technology
Rm. 36-351
Cambridge, MA 02139

Dr. S. Hawkins
Lawrence Livermore National Laboratory
P. O. Box 808
Livermore, CA 94550

Dr. Carl Hess
MS B-118
VARIAN
611 Hanson Way
Palo Alto, CA 94303

Dr. J. L. Hirshfield (2 copies)
Yale University
Mason Laboratory
400 Temple Street
New Haven, CT 06520

Dr. K. Hizanidis
Physics Dept.
University of Maryland
College Park, MD 20742

Dr. A. H. Ho
Dept. of Electrical Engineering
Stanford University
Stanford, CA 94305

Dr. Darwin Ho
L-477
Lawrence Livermore National Laboratory
P. O. Box 808
Livermore, CA 94550

Dr. J. Hoffman
Sandia National Laboratories
ORG. 1231, P.O. Box 5800
Albuquerque, NM 87185

Dr. R. Hofland
Aerospace Corp.
P. O. Box 92957
Los Angeles, CA 90009

Dr. Fred Hopf
Optical Sciences Building, Room 602
University of Arizona
Tucson, AZ 85721

Dr. Heinrich Hora
Iowa Laser Facility
University of Iowa
Iowa City, Iowa

Dr. J. Y. Hsu
General Atomic
San Diego, CA 92138

Dr. H. Hsuan
Princeton Plasma Physics Lab.
James Forrestal Campus
P.O. Box 451
Princeton, NJ 08544

Dr. James Hu
Quantum Inst. and Phys. Dept.
University of California
Santa Barbara, CA 93106

Dr. Benjamin Hubberman
Associate Director, OSTP
Rm. 476, Old Executive Office Bldg.
Washington, DC 20506

Dr. J. Hyman
Hughes Research Laboratory
3011 Malibu Canyon Road
Malibu, CA 90265

Dr. H. Ishizuka
University of California
Department of Physics
Irvine, CA 92717

Dr. A. Jackson
Lawrence Berkeley Laboratory
University of California, Berkeley
Berkeley, CA 94720

Dr. S. F. Jacobs
Optical Sciences Center
University of Arizona
Tucson, AZ 85721

Dr. Pravin C. Jain
Asst. for Communications Tech.
Defense Communications Agency
Washington, DC 20305

Dr. E. T. Jaynes
Physics Department
Washington University
St. Louis, MO 63130

Dr. B. Carol Johnson
Ctr. for Radiation Research
National Bureau of Standards
Gaithersburg, MD 20899

Dr. Bernadette Johnson
Lincoln Laboratory
Lexington, MA 02173

Dr. Richard Johnson
Physics International
2700 Merced St.
San Leandro, CA 94577

Dr. G. L. Johnston
NW 16-232
Mass. Institute of Tech.
Cambridge, MA 02139

Dr. Shayne Johnston
Physics Department
Jackson State University
Jackson, MS 39217

Dr. William Jones
U. S. Army SDC
P. O. Box 1500
Huntsville, AL 35807-3801

Dr. R. A. Jong
Lawrence Livermore National Laboratory
P. O. Box 808/L626
Livermore, CA 94550

Dr. Howard Jory (3 copies)
Varian Associates, Bldg. 1
611 Hansen Way
Palo Alto, CA 94303

Dr. C. Joshi
University of California
Los Angeles, CA 90024

Dr. Paul Kennedy
Rockwell International/Rocketdyne Div.
6633 Canoga Avenue, FA-40
Canoga Park, CA 91304

Dr. R. Kennedy
Boeing Aerospace Company
P.O. Box 3999
Seattle, WA 98124

Dr. K. J. Kim, MS-101
Lawrence Berkeley Lab.
Rm. 223, B-80
Berkeley, CA 94720

Dr. I. Kimel
Creol-FEL Research Pavillion
Suite 400
12424 Research Parkway
Orlando, FL 32826

Dr. Brian Kincaid
Lawrence Berkeley Laboratory
University of California, Berkeley
Berkeley, CA 94720

Dr. S. P. Kno
Polytechnic Institute of NY
Route 110
Farmingdale, NY 11735

Dr. Xu Knogyi
Room 36-285
Mass. Institute of Technology
Cambridge MA 02139

Dr. A. Kolb
Maxwell Laboratories, Inc.
8835 Balboa Avenue
San Diego, CA 92123

Dr. Eugene Kopf
Principal Deputy Assistant
Secretary of the Air Force (RD&L)
Room 4E964, The Pentagon
Washington, D.C. 20330

Dr. P. Korn
Maxwell Laboratories, INC.
8835 Balboa Avenue
San Diego, CA 92123

Dr. S. Krinsky
Nat. Synchrotron Light Source
Brookhaven National Laboratory
Upton, NY 11973

Prof. N. M. Kroll
Department of Physics
B-019, UCSD
La Jolla, CA 92093

Dr. Thomas Kwan
Los Alamos National Scientific
Laboratory, MS608
P. O. Box 1663
Los Alamos, NM 87545

Dr. Jean Labacqz
Stanford University
SLAC
Stanford, CA 94305

Dr. Ross H. Labbe
Rockwell International/Rocketdyne Div.
6633 Canoga Avenue, FA-40
Canoga Park, CA 91304

Dr. Willis Lamb
Optical Sciences Center
University of Arizona
Tucson, AZ 85721

Dr. H. Lancaster
Lawrence Berkeley Laboratory
University of California, Berkeley
Berkeley, CA 94720

Dr. D. J. Larson
The Inst. for Accelerator Physics
Department of Physics
University of Wisconsin-Madison
Madison, WI 53706

Dr. J. LaSala
Physics Dept.
U. S. M. A.
West Point, NY 10996

Dr. Bernard Laskowski
M.S. 230-3
NASA-Ames
Moffett Field, CA 94305

Dr. Charles J. Lasnier
TRW
High Energy Physics Lab.
Stanford University
Stanford, CA 94305

Dr. Michael Lavan
U.S. Army Strategic Def. Command
ATTN: Code CSSD-H-D
P. O. Box 1500
Huntsville, AL 35807-3801

Dr. Ray Leadabrand
SRI International
333 Ravenswood Avenue
Menlo Park, CA 94025

Dr. Kotik K. Lee
Perkin-Elmer
Optical Group
100 Wooster Heights Road
Danbury, CT 06810

Dr. K. Lee
Los Alamos Nat. Scientific Lab.
Attn: X-1 MS-E531
P. O. Box 1663
Los Alamos, NM 87545

Dr. Barry Leven
NISC/Code 20
4301 Suitland Road
Washington, D.C. 20390

Dr. B. Levush
Dept. of Physics & Astronomy
University of Maryland
College Park, MD 20742

Dr. Lewis Licht
Department of Physics
Box 4348
U. of Illinois at Chicago Cir.
Chicago, IL 60680

Dr. M. A. Lieberman
Dept. EECS
Univ. of Cal. at Berkeley
Berkeley, CA 94720

Dr. Anthony T. Lin
Dept. of Physics
University of California
Los Angeles, CA 90024

Dr. B. A. Lippmann
Stanford Linear Accel. Center
BIN 26
Stanford, CA 94305

Dr. Chuan S. Liu
Dept. of Physics & Astronomy
University of Maryland
College Park, MD 20742

Dr. R. Lohsen
Los Alamos National Laboratory
P. O. Box 1663
Los Alamos, NM 87545

Dr. D. D. Lowenthal
Spectra Technology
2755 Northup Way
Bellevue, WA 98004

Dr. A. Luccio
Brookhaven National Laboratory
Accelerator Dept.
Upton, NY 11973

Dr. A. Lumpkin
Los Alamos National Laboratory
P. O. Box 1663
Los Alamos, NM 87545

Dr. Phil Mace
W. J. Shafer Assoc., Inc.
1901 N. Fort Myer Drive
Arlington, VA 22209

Prof. J.M.J. Madey
Stanford University
Stanford Photon Research Lab.
Stanford, CA 94305-4087

Dr. R. Mako
FM Technologies Corp.
6308 Youngs Branch Dr.
Fairfax Station, VA 22039

Dr. Joseph Mangano
Science Research Laboratory
1600 Wilson Blvd.
Suite 1200
Arlington, VA 22209

Dr. Siva A. Mani
Science Applications Intl. Corp.
1040 Waltham Street
Lexington, MA 02173-8027

Dr. J. Mark
Lawrence Livermore National Lab.
Attn: L-477
P. O. Box 808
Livermore, CA 94550

Dr. T. C. Marshall
Applied Physics Department
Columbia University
New York, NY 10027

Dr. Xavier K. Maruyama
Dept. of Physics
Naval Postgraduate School
Monterey, CA 93943

Dr. Neville Marzwell
Jet Propulsion Lab.
MS 198-330
4800 Oak Grove Drive
Pasadena, CA 91109

Dr. A. Maschke
TRW
Mail Stop 01-1010
1 Space Park
Redondo Beach CA 90278

Dr. Joseph Mathew
Sachs/Freeman Associates
14300 Gallant Fox Lane
Bowie, MD 20715

Dr. K. Matsuda
GA Technologies Inc.
P.O. Box 85608
San Diego, CA 92138

Dr. John McAdoo
Mission Research Corporation
5503 Cherokee Ave., Suite 201
Alexandria, VA 22312

Dr. D. B. McDermott
Electrical Engineering Dept.
University of California
Los Angeles, CA 90024

Dr. J. K. McIver
Dept. of Physics & Astronomy
Univ. of New Mexico
800 Yale Blvd. NE
Albuquerque, NM 87131

Dr. C. McKinstrie
MS B258
P.O. Box 1663
Los Alamos, NM 87545

Dr. B. McVey
Los Alamos National Laboratory
P. O. Box 1663
Los Alamos, NM 87545

Dr. John Meson
DARPA
1400 Wilson Boulevard
Arlington, VA 22209

Col Thomas Meyer
SDIO/DEO
The Pentagon, Rm. 1E180
Washington, DC 20301-7100

Dr. F. E. Mills
Fermilab
P.O., Box 500
Batavia, IL 60510

Dr. D. R. Mize
Hughes Research Laboratory
3011 Malibu Canyon Road
Malibu, CA 90265

Dr. Mel Month
Brookhaven National Laboratories
Associated Universities, Inc.
Upton, L.I., NY 11973

Dr. B. N. Moore
Austin Research Assoc.
1901 Rutland Dr.
Austin, TX 78758

Dr. Gerald T. Moore
University of New Mexico
Albuquerque, NM 87131

Dr. Warren Mori
1-130 Knudsen Hall
U.C.L.A.
Los Angeles, CA 90024

Dr. Philip Morton
Stanford Linear Accelerator Center
P.O. Box 4349
Stanford, CA 94305

Dr. Jesper Munch
TRW
One Space Park
Redondo Beach, CA 90278

Dr. James S. Murphy
National Synchrotron Light Source
Brookhaven National Laboratory
Upton, NY 11975

Dr. J. Nation
224 Phillips Hall
School of Elec. Eng.
Cornell University
Ithaca, NY 14850

Dr. R. Neighbours
Physics Department
Naval Postgraduate School
Monterey, CA 93943

Dr. George Neil
TRW
One Space Park
Redondo Beach, CA 90278

Dr. Kelvin Neil
Lawrence Livermore National Lab.
Code L-321, P.O. Box 808
Livermore, CA 94550

Dr. W. M. Nevins
L-639
Lawrence Livermore National Laboratory
P. O. Box 808
Livermore, CA 94550

Dr. Brian Newnam
MSJ 564
Los Alamos National Scientific Lab.
P.O. Box 1663
Los Alamos, NM 87545

Dr. W. Nexsen
Lawrence Livermore National Laboratory
P. O. Box 808
Livermore, CA 94550

Lt. Rich Nielson/ESD/INK
Hanscomb Air Force Base
Stop 21, MA 01731

Dr. Milton L. Noble (2 copies)
General Electric Company
G. E. Electric Park
Syracuse, NY 13201

Dr. K. O'Brien
Div. 1241 SNLA
Albuquerque, NM 87185

Dr. John D. O'Keefe
TRW
One Space Park
Redondo Beach, CA 90278

Dr. T. Orzechowski
L-436
Lawrence Livermore National Lab.
P. O. Box 808
Livermore, CA 94550

Prof. E. Ott (2 copies)
Department of Physics
University of Maryland
College Park, MD 20742

OUSDRE (R&AT)
Room 3D1067, The Pentagon
Washington, D.C. 20301

Dr. A. J. Palmer
Hughes Research Laboratory
3011 Malibu Canyon Road
Malibu, CA 90265

Dr. Robert B. Palmer
Brookhaven National Laboratories
Associated Universities, Inc.
Upton, L.I., NY 11973

Dr. J. Palmer
Hughes Research Laboratory
Malibu, CA 90265

Dr. Richard H. Pantell
Stanford University
Stanford, CA 94305

Dr. Dennis Papadopoulos
Astronomy Department
University of Maryland
College Park, Md. 20742

Dr. P. Parks
GA Technologies
P.O. Box 85608
San Diego, Ca 92138

Dr. John A. Pasour
Mission Research Laboratory
8560 Cinderbed Road
Suite 700
Newington, VA 22122

Dr. C. K. N. Patel
Bell Laboratories
Murray Hill, NJ 07974

Dr. Richard M. Patrick
AVCO Everett Research Lab., Inc.
2385 Revere Beach Parkway
Everett, MA 02149

Dr. Claudio Pellegrini
Brookhaven National Laboratory
Associated Universities, Inc.
Upton, L.I., NY 11973

Dr. S. Penner
Center for Radiation Research
National Bureau of Standards
Gaithersburg, MD 20899

Dr. D. E. Pershing
Mission Research Corporation
5503 Cherokee Avenue
Alexandria, VA 22312

Dr. J. M. Peterson
Lawrence Berkeley Laboratory
University of California, Berkeley
Berkeley, CA 94720

Dr. M. Piestrup
Adelphi Technology
13800 Skyline Blvd. No. 2
Woodside, CA 94062

Dr. Alan Pike
DARPA
1400 Wilson Boulevard
Arlington, VA 22209

Dr. Hersch Pilloff
Code 421
Office of Naval Research
Arlington, VA 22217

Dr. A. L. Pindroh
Spectra Technology
2755 Northup Way
Bellevue, WA 98004

Dr. D. J. Pistoresi
Boeing Aerospace Company
P. O. Box 3999
Seattle, WA 98124-2499

Major E. W. Pogue
SDIO
The Pentagon, T-DE Rm. 1E180
Washington, DC 20301-7100

Dr. Peter Politzer
General Atomic Tech., Rm. 13/260
P. O. Box 85608
San Diego, CA 92138

Major Donald Ponikvar
U. S. Army SDC
P. O. Box 15280
Arlington, VA 22245-0280

Dr. S. E. Poor
Lawrence Livermore National Laboratory
P. O. Box 808
Livermore, CA 94550

Prof. M. Porkolab
NW 36-213
Mass. Institute of Technology
Cambridge, MA 02139

Dr. R. V. Pound
Physics Department
Harvard University
Cambridge, MA 02138

Mr. J. E. Powell
Sandia National Laboratories
ORG. 1231, P.O. Box 5800
Albuquerque, NM 87185

Dr. Anand Prakash
Ballistic Research Laboratory
Aberdeen Proving Ground, MD 21005

Dr. Mark A. Prelas
Nuclear Engineering
Univ. of Missouri-Columbia
1033 Engineering
Columbia, Missouri 65211

Dr. Donald Prosnitz
Lawrence Livermore National Lab.
Box 5511 L-626
Livermore, CA 94550

Dr. D. C. Quimby
Spectra Technology
2755 Northup Way
Bellevue, WA 98004

Dr. Paul Rabinowitz
Xerox Research and Eng. Comp.
P. O. Box 45
Linden, NJ 07036

Dr. G. Ramian
Quantum Institute
University of California
Santa Barbara, CA 93106

Dr. L. Ranjun
Dept. of Physics
University of Cal. at Irvine
Irvine, CA 92717

Dr. L. L. Reginato
Lawrence Livermore National Laboratory
P. O. Box 808
Livermore, CA 94550

Dr. M. B. Reid
Dept. of Electrical Engineering
Stanford University
Stanford, CA 94305

Dr. D. A. Reilly
AVCO Everett Research Lab.
Everett, MA 02149

Dr. M. Reiser
University of Maryland
Department of Physics
College Park, MD 20742

Dr. S. Ride
Arms Control
Stanford University
Stanford, CA 94305

Dr. C. W. Roberson
Office of Naval Research
Code 112S
800 N. Quincy Street
Arlington, VA 22217

Dr. B. Robinson
Boeing Aerospace Company
P.O. Box 3999
Seattle, WA 98124

Dr. K. Robinson
Spectra Technology
2755 Northup Way
Bellevue, WA 98004

Dr. D. Rogers
Lawrence Livermore National Laboratory
P. O. Box 808
Livermore, CA 94550

Dr. Jake Romero
Boeing Aerospace Company
P. O. Box 3999
Seattle, WA 98124-2499

Dr. T. Romesser
TRW, Inc.
One Space Park
Redondo Beach, Ca 90278

Dr. Marshall N. Rosenbluth
Institute for Fusion Studies
The Univ. of Texas at Austin
Austin, TX 78712

Dr. J. B. Rosenzweig
The Inst. for Accelerator Physics
Department of Physics
University of Wisconsin-Madison
Madison, WI 53706

Dr. J. Ross
Spectra Technology
2755 Northup Way
Bellevue, WA 98004

Dr. N. Rostoker
Department of Physics
University of California at Irvine
Irvine, CA 92717

Dr. G. A. Saenz
Hughes Research Laboratory
3011 Malibu Canyon Road
Malibu, CA 90265

Dr. Antonio Sanchez
Lincoln Laboratory
Mass. Institute of Tech.
Room B213
P. O. Box 73
Lexington, MA 02173

Dr. Aldric Saucier
BMD-PO
Ballistic Missile Defense
Program Office
P. O. Box 15280
Arlington, VA 22215

Dr. A. Saxman
Los Alamos National Scientific Lab.
P. O. Box 1663, MSE523
Los Alamos, NM 87545

Dr. J. Scharer
ECE Dept.
Univ. of Wisconsin
Madison, WI 53706

Dr. E. T. Scharlemann
L626
Lawrence Livermore National Laboratory
P. O. Box 808
Livermore, CA 94550

Prof. S. P. Schlesinger
Dept. of Electrical Engineering
Columbia University
New York, NY 10027

Dr. Howard Schlossberg
AFOSR
Bolling AFB
Washington, D.C. 20332

Dr. George Schmidt
Stevens Institute of Technology
Physics Department
Hoboken, NJ 07030

Dr. M. J. Schmitt
Los Alamos National Laboratory
P. O. Box 1663
Los Alamos, NM 87545

Dr. Stanley Schneider
Rotodyne Corporation
26628 Fond Du Lac Road
Palos Verdes Peninsula, CA 90274

Dr. N. Schoen
TRW DSSG
One Space Park
Redondo Beach, CA 90278

Dr. M. L. Scott
Los Alamos National Laboratory
P. O. Box 1663
Los Alamos, NM 87545

Dr. Richard L. Schrieffer (DP-23)
Director, Office of Inertial Fusion
U. S. Department of Energy
Washington, D.C. 20545

Dr. R. W. Schumacher
Hughes Research Laboratories
3011 Malibu Canyon Road
Malibu, CA 90265

Dr. H. Schwettmann
Phys. Dept. & High Energy
Physics Laboratory
Stanford University
Stanford, CA 94305

Dr. Marlan O. Scully
Dept. of Physics & Astronomy
Univ. of New Mexico
800 Yale Blvd. NE
Albuquerque, NM 87131

Dr. S. B. Segall
KMS Fusion
3941 Research Park Dr.
P.O. Box 1567
Ann Arbor, MI 48106

Dr. Robert Sepucha
DARPA
1400 Wilson Boulevard
Arlington, VA 22209

Prof. P. Serafim
Northeastern University
Boston, MA 02115

Dr. A. M. Sessler
Lawrence Berkeley Laboratory
University of California
1 Cyclotron Road
Berkeley, CA 94720

Dr. W. Sharp
L-626
Lawrence Livermore National Laboratory
P. O. Box 808
Livermore, CA 94550

Dr. Earl D. Shaw
Bell Laboratories
600 Mountain Avenue
Murray Hill, NJ 07974

Dr. J. P. Sheerim
KMS Fusion
P.O. Box 1567
Ann Arbor, MI 48106

Dr. R. Shefer
Science Research Laboratory
15 Ward Street
Somerville, MA 02143

Dr. R. L. Sheffield
Los Alamos National Laboratory
P.O. Box 1663
Los Alamos, NM 87545

Dr. Shemwall
Spectra Technology
2755 Northup Way
Bellevue, WA 98004

Dr. Shen Shey
DARPA/DEO
1400 Wilson Boulevard
Arlington, VA 22209

Dr. D. Shoffstall
Boeing Aerospace Company
P.O. Box 3999
Seattle, WA 98124

Dr. I. Shokair
SNLA, Org. 1271
Albuquerque, NM 87185

Dr. J. S. Silverstein
Harry Diamond Laboratories
2800 Powder Mill Road.
Adelphi, MD 20783

Dr. Jack Slater
Spectra Technology
2755 Northup Way
Bellevue, WA 98004

Dr. Kenneth Smith
Physical Dynamics, Inc.
P.O. Box 556
La Jolla, CA 92038

Dr. Lloyd Smith
Lawrence Berkeley Laboratory
University of California
1 Cyclotron Road
Berkeley, CA 94720

Dr. Stephen J. Smith
JILA
Boulder, CO 80302

Dr. T. Smith
TRW, Inc.
One Apaca Park
Redondo Beach, CA 90278 R1/2044

Dr. Todd Smith
Hansen Labs
Stanford University
Stanford, CA 94305

Dr. J. Z. Soln (22300)
Harry Diamond Laboratories
2800 Powder Mill Road
Adelphi, MD 20783

Dr. G. Spalek
Los Alamos National Laboratory
P. O. Box 1663
Los Alamos, NM 87545

Dr. Richard Spitzer
Stanford Linear Accelerator Center
P.O. Box 4347
Stanford, CA 94305

Mrs. Alma Spring
DARPA/Administration
1400 Wilson Boulevard
Arlington, VA 22209

SRI/MP Reports Area G037 (2 copies)
ATTN: D. Leitner
333 Ravenswood Avenue
Menlo Park, CA 94025

Dr. W. Stein
Los Alamos National Laboratory
P. O. Box 1663
Los Alamos, NM 87545

Dr. L. Steinhauer
STI
2755 Northup Way
Bellevue, WA 98004

Dr. Efrem J. Sternbach
Lawrence Berkeley Laboratory
University of California, Berkeley
Berkeley, CA 94720

Dr. M. Strauss
Department of Physics
University of California at Irvine
Irvine, CA 92717

Dr. W. C. Stwalley
Iowa Laser Facility
University of Iowa
Iowa City, Iowa 52242

Dr. R. Sudan
Lab. of Plasma Studies
Cornell University
Ithaca, NY 14850

Dr. P. W. Sumner
Hughes Research Laboratory
3011 Malibu Canyon Road
Malibu, CA 90265

Dr. David F. Sutter
ER 224, GTN
Department of Energy
Washington, D.C. 20545

Dr. Abraham Szoke
ML/L-470
Lawrence Livermore Natl. Lab.
P.O. Box 808
Livermore, CA 94550

Dr. R. Taber
Dept. of Phys. & High Energy Lab.
Stanford University
Stanford, CA 94305

Dr. T. Tajima
Institute for Fusion Studies
University of Texas at Austin
Austin, TX 78712

Dr. H. Takeda
Los Alamos National Laboratory
P. O. Box 1663
Los Alamos, NM 87545

Dr. J. J. Tancredi
Hughes Aircraft Co.
Electron Dynamics Division
3100 West Lomita Blvd.
Torrance, CA 90509

Dr. Milan Tekula
AVCO Everett Research Lab.
2385 Revere Beach Parkway
Everett, MA 02149

Dr. R. Temkin (2 copies)
Mass. Institute of Technology
Plasma Fusion Center
Cambridge, MA 02139

Dr. L. Thode
Los Alamos National Laboratory
P. O. Box 1663
Los Alamos, NM 87545

Dr. Keith Thomassen, L-637
Lawrence Livermore National Laboratory
P. O. Box 808
Livermore, CA 94550

Dr. Harold Thompson
TRW, Inc.
R1/2120
One Space Park
Redondo Beach, Ca 90278

Dr. Norman H. Tolk
Physics Department
Vanderbilt University
Nashville, TN 37240

Dr. Kang Tsang
Science Applications Intl. Corp.
10260 Campus Point Drive
San Diego, CA 92121

Dr. E. Tyson
Boeing Aerospace Company
P.O. Box 3999
Seattle, WA 98124

Dr. H. S. Uhm
Naval Surface Warfare Center
White Oak Lab.
Silver Spring, MD 20903-5000

Dr. L. Ulstrup
TRW, Inc.
One Space Park
Redondo Beach, Ca 90278

Under Secretary of Defense (R&D)
Office of the Secretary of Defense
Room 3E1006, The Pentagon
Washington, D.C. 20301

Dr. L. Vahala
Physics Dept.
College of William & Mary
Williamsburg, VA 23185

Dr. A. Valla
Spectra Technology
2755 Northup Way
Bellevue, WA 98004

Dr. A. Vetter
Boeing Aerospace Company
P.O. Box 3999
Seattle, WA 98124

Dr. A. A. Vetter
Spectra Technology
2755 Northup Way
Bellevue, WA 98004

Dr. G. Vignola
Brookhaven National Laboratories
Associated Universities, Inc.
Upton, L.I., NY 11973

Dr. S. A. Von Laven
KMS Fusion Inc.
Ann Arbor, MI 48106

Dr. John E. Walsh
Wilder Laboratory
Department of Physics (HB 6127)
Dartmouth College
Hanover NH 03755

Dr. W. M. Walsh, Jr.
Bell Laboratories
600 Mountain Avenue
Room 1-D 332
Murray Hill, NJ 07974

Dr. Jiunn-Ming Wang
Brookhaven National Laboratories
Associated Universities, Inc.
Upton, L.I., NY 11973

Dr. T-S. Wang
Los Alamos National Laboratory
P. O. Box 1663
Los Alamos, NM 87545

Dr. J. F. Ward
University of Michigan
Ann Arbor, MI 48109

Dr. E. Warden
Code PDE 106-3113
Naval Electronics Systems Command
Washington, DC 20363

Dr. Roger W. Warren
Los Alamos National Scientific Lab.
P.O. Box 1663
Los Alamos, NM 87545

Dr. J. Watson
Los Alamos National Laboratory
P. O. Box 1663
Los Alamos, NM 87545

Dr. B. Weber
Harry Diamond Laboratories
2800 Powder Mill Road
Adelphi, MD 20783

Dr. Lee Webster
BMD/ATC
Box 1500
Huntsville, AL 35807

Dr. J. T. Weir
Lawrence Livermore National Laboratory
P. O. Box 808
Livermore, CA 94550

Dr. R. Whitefield
15260 Dickens Ave.
San Jose, CA 95124

Ms. Bettie Wilcox
Lawrence Livermore National Lab.
ATTN: Tech. Info. Dept. L-3
P.O. Box 808
Livermore, CA 94550

Dr. Mark Wilson
National Bureau of Standards
Bldg. 245, Rm. B-119
Gaithersburg, MD 20899

Dr. H. Winick
Stanford Synch. Rad. Lab.
SLAC Bin 69
P.O. Box 44349
Stanford, CA 94550

Dr. J. Workman
Berkeley Research Associates
P.O. Box 241
Berkeley, CA 94701

Dr. Jack Wong (L-71)
Lawrence Livermore National Lab.
P. O. Box 808
Livermore, CA 94550

Dr. Thomas P. Wright
Sandia National Laboratories
ORG. 1231, P.O. Box 5800
Albuquerque, NM 87185

Dr. J. Wurtele
M.I.T.
NW 16-234
Plasma Fusion Center
Cambridge, MA 02139

Dr. Ming Xie
Dept. of Physics
Stanford University
Stanford, CA 94305

Dr. Edward Yadlowsky
High-Tech Research
P. O. Box 3422
Radford, VA 24143

Dr. Yi-Ton Yan
MS-B259
Los Alamos National Lab.
Los Alamos, NM 87545

Dr. A. Yariv
California Institute of Tech.
Pasadena, CA 91125

Dr. J. Yeh
Allied Corporation
31717 La Tienda Dr.
Westlake Village, CA 91362

Dr. A. Yeremian
Boeing Aerospace Company
P.O. Box 3999
Seattle, WA 98124

Dr. Barbara Yoou
R & D Associates
1401 Wilson Blvd., Suite 500
Arlington, VA 22209

Dr. Li Hua Yu
725B, NSLS
Brookhaven National Laboratory
Upton, NY 11973

Dr. Simon S. Yu
Lawrence Livermore National Laboratory
P. O. Box 808
Livermore, CA 94550

Dr. Mark Zedikev
103 S. Goodwin
Urbana, IL 61801

Dr. M. S. Zisman
Lawrence Berkeley Laboratory
University of California, Berkeley
Berkeley, CA 94720

Dr. J. Zumdieck
Spectra Technology
2755 Northup Way
Bellevue, WA 98004